IMAGE-BASED TISSUE INFORMATICS – TAA INDUCED HEPATOTOXICITY MODEL

SHAO LIN

NATIONAL UNIVERSITY OF SINGAPORE

2007

IMAGE-BASED TISSUE INFORMATICS – TAA INDUCED HEPATOTOXICITY MODEL

SHAO LIN
(B. ENG., XJTU, China)

A THESIS SUBMITTED

FOR THE DEGREE OF MASTER OF SCIENCE

DEPARTMENT OF BIOLOGICAL SCIENCE

NATIONAL UNIVERSITY OF SINGAPORE

2007

THESIS ADVISORS:

PROFESSOR HEW CHOY LEONG

ACKNOWLEDGEMENTS

I would very much like to thank my advisor, Prof. Hew Choy Leong, and committee members of the Computation and Systems Biology program, who give me the chance for finishing my masters' thesis. I would also like to thank Singapore-MIT Alliance for the financial support of my research.

I would like to thank, Dr. Hanry Yu, for his supervision and encouragement of my graduate study. I would also like to acknowledge Dr. Hong Yunhan and Dr. Peter So, who have offered their time and expertise to assist in the evaluation of my research.

I would like to extent my gratitude to all the lab members in Institute of Bioengineering and Nanotechnology and Clinic Research Center, who have always been willing to share their time by answering questions or providing spiritual support.

Last, I would especially like to thank my parents and friends, for all of their love and support.

TABLE OF CONTENTS

Page Numbers

SUMMARY

Hepatotoxicity is chemical-driven liver damage. It is a common side-effect of certain medications. It can also be caused by chemicals used in laboratories and industry, and natural chemicals. In the drug development industry, over 90% of the market withdrawals were caused by drug toxicity. Hepatic toxicity seems to be the major problem among the drug toxicity. Hepatotoxicity accounts for near 30% of drug withdrawn from the market during 1960 – 2002. And hepatotoxicity also accounts for over 40% of drug candidate terminations in clinical phase. The pharmaceutical companies estimate that clinical failure due to hepatotoxicity cost more than $2 billion dollars in lost revenue in the past ten years (Schuster et al, 2005).

Drug discovery involves a complex iterative process of biochemical and cellular assays, with final validation in animal models, and ultimately in humans. Mammalian models of absorption, distribution, metabolism and excretion (ADME)/pharmacokinetics and efficacy are expensive, laborious and consume large quantities of precious compounds. There is also increasing pressure to limit animal use to situations in which they are absolutely necessary, such as in preclinical toxicity and safety assessment. In the past few decades, zebrafish are beginning to be used at various stages of the drug discovery process and can be a useful and cost-effective alternative to some mammalian models (such as rodents, dogs and pigs) (Zon and Peterson, 2005). Zebrafish is one of the small teleost fish that has long been a favorite in home aquariums due to its hardy nature, has

emerged as one of the leading models for studying development. As a vertebrate organism, the zebrafish presents many organs and cell types similar to that of mammals.

Like the zebrafish, the medaka, *Oryzias latipes*, is another fish model with similar features (Wittbrodt, 2002). In this thesis, we aimed to establish an in vivo model for the screening of hepatotoxicity using medaka fish. Thioacetamide, a commonly used model toxin for the study of hepatotoxicity, hepatocarcinogenicity and cellular response to injury, was used for the production of hepatic lesion in medaka fish. The most effective thioacetamide concentrations for chronic and acute liver damage were determined by a series of treatments. RT-PCR and H&E staining methods were used to examine the mRNA expression level of several genes and the architecture of tissue in damaged liver. In order to extract more information from the tissue and to make the information more quantitative, we have developed and applied Two-Photon Excitation Fluorescence/ Second Harmonic Generation Microscopy for imaging of unstained liver tissue. Quantitative signals were obtained from hepatocytes and extracellular matrix. Comprehensive imaging processing algorithms were developed for quantification of collagen content and cell necrosis. At last, the whole liver of liver-RFP transgenic fish was imaged under Two-photon Excitation Fluorescence microcopy without sectioning. Subcellular resolution was obtained for the deep tissue imaging. Then the imaging depth of nonlinear microscopy was investigated in optically cleared and fresh frozen muscle tissue. This study will help to improve penetration capability for 3D imaging and reconstruction of whole organ in the future.

LIST OF TABLES

LIST OF FIGURES

LIST OF ABBREVIATIONS

- **TAA** Thioacetamide
- **HTS** High-Throughput Screening
- **CCl_4** Carbon Tetrachloride
- **DMN** Dimethylnitrosamine
- **TPEF** Two-photon Excitation Fluorescence
- **SHG** Second Harmornic Generation
- **ECM** extracellular matrix
- **PCR** Polymerase Chain Reaction
- **O.C.T.** optical cutting temperature compound
- **H&E** Hematoxylin and Eosin
- **VBAT** venous-biliary-arteriolar tracts
- **VAT** venous-arteriolar tracts
- **BAT** biliary-arteriolar tracts
- **VBT** venous-biliary tracts
- **BT** biliary tracts
- **AT** arteriolar tracts
- **L-FABP** liver-type fatty acid binding protein
- **RFP** red fluorescence protein

CHAPTER 1 INTRODUCTION

1.1 Medaka as a research model organism

Medaka, *Oryzias latipes*, is native to Asia mainly in Japan, Korea and China. It is a small (3 cm to 4 cm), egg-laying freshwater fish. It has a short generation time of 2 to 3 months. Males and females are easily distinguished by their external secondary sex characters such as the shape and size of the anal and dorsal fins. The fish produce fully transparent eggs daily (30 to 50 eggs per day) that develop synchronously. The eggs can be staged under dissecting microscope to study early developmental process. Medaka is a hardy animal that can reproduce successfully under microgravity conditions in a space shuttle (Ijiri, 1995) and withstand a wide range of salinity and temperatures. Tolerable temperature ranges from as low as 3 ^{o}C to 38 ^{o}C. The optimum temperature for breeding lies between 25 ^{o}C to 28 ^{o}C, and if maintained at this temperature, spawning can be induced simply by the light cycles (14 h light and 10 h dark). In addition, early medaka embryos can be maintained at temperatures as low as 4 ^{o}C to slow down their development for several days without affecting normal development. With the ease of breeding and low susceptibility to common fish diseases, the maintenance of the medaka is easy, cheap and not space consuming.

Medaka is a useful animal model to investigate waste water toxicology (Ma et al., 2005), endocrine disruptors (Scholz et al., 2004), liver carcinogenesis (Liu et al., 2003), germ cell mutagenesis (Shimada et al, 2005), gene mutagenesis (Winn et al, 2005), and developmental and functional genomics (Ju et al, 2005). Small fish such as medaka and

zebrafish have attracted much interest as valuable vertebrate models for organogenesis and human disease since they have organs and tissues that are functionally equivalent to those of mammals (Zon and Peterson, 2005). Their small size allows for large numbers to be exposed to small amounts of chemicals, thus allowing statistical analysis. In addition, the whole organ can be isolated for RNA isolation and histological studies. Sections from one or more bisected fish can all be placed on few slides, to decrease costs, allow examination of almost all major organ systems and accelerate histological evaluation. Finally, medaka liver is small (2x2x3 mm) and solid (no lobes), ideal for morphometric evaluation. For example, Steatohepatitis in zebrafish embryos using thioacetamide (TAA) has been induced (Amali et al, 2006). These investigations have observed significant increase of apoptosis, accumulation of fatty droplets, and up-regulation of apoptotic genes and steatosis markers in liver.

Another big advantage of using small fish as disease model is that their embryo and larvae are well suited to high-throughput screening (HTS) (Zon and Peterson, 2005). The embryo and larvae are optically transparent, making it possible to detect functional and morphological changes in internal organs without having to kill or dissect the organism. These functional and morphological changes can be further highlighted by the use of transgenic lines and other reporter molecules, which can be easily produced in fish. For example, fluorescently quenched phospholipids were used to detect lipid processing and transport in live, intact zebrafish (Farber et al, 2001). The transparent fish and fluorescent marker were combined to facilitate the rapid phenotyping of thousands of individuals in a large-scale screening for genes that affect lipid trafficking.

1.2 Liver anatomy of teleost fish

Certain features of the hepatic gross and microscopic anatomy of fish are different from those of mammalian liver. There are important considerations in the context of organ toxicity (Hinton et al, 2001).

First, fish livers are in the form of a single lobe, whereas livers of mammals have multiple lobes. Second, the classic lobule, a consistent microscopic feature of mammalian liver, is not present in fish. Portal tracts found at corners of the classic lobule in mammals are delimited by perilobular connective tissue and contain bile duct, portal venule and hepatic arteriole. In fish liver, no bile ducts or hepatic arterioles are in close association and no tissue components analogous to portal tracts of rodent liver were present. Portal tracts indicate sites where arterial blood enters hepatic sinusoids supplying hepatocytes at the periphery of hepatic lobules with oxygenated blood. Cytologic features of hepatocytes at the periphery of lobules differ from those of hepatocytes at the center of the classic lobule. Exposure of rodents to certain reference hepatotoxicants resulted in a mosaic of altered and unaltered parenchyma, depending on the targeting of afferent or efferent zones by the toxicant. However, no such pattern can be observed in fish liver. The metabolic zonation within the mammalian liver lobule does not exist in fish. Third, hepatocytes are typically arranged as laminae, one hepatocyte thick, resulting in both lateral plasma membranes of individual hepatocytes in close proximity to the microcirculation. However, microscopic analysis of trout liver sections reveals a double row of hepatocytes. Thus, only one surface of the teleost hepatocyte will face the sinusoid. This tubular architectural pattern of fish may result in different rates of uptake of

endogenous compounds and xenobiotics. Another important difference between mammalian liver and that of fish is the fixed macrophage of the mammalian sinusoids, the Kupffer cells, are absent in most teleosts. Perisinusoidal, interhepatocytic macrophges are occasionally present in mammals, but are apparently much more common in livers of fish (Hinton et al, 2001).

The liver is a glucose-utilizing, glucose-producing and glucose-storing organ. It acts as a glucostat in the vertebrate organism, regulating glucose levels of blood. When glycemia is challenged, the liver elicits adaptive metabolic responses, thereby maintaining a level of blood glucose which is optimal for animal function. Glycemic levels and glucose turnover rates of fish are 20-100 times lower than those for mammals of equivalent size. The lower body temperature and lower metabolic rate of fish may account for this difference. Hepatic removal of excess glucose from the blood is comparatively inefficient in teleost fish. The diabetic-like behavior of fish is related to a low hepatic capacity for glucose uptake, rather than a lack of insulin or insulin receptors (Hinton et al, 2001).

1.3 Toxic responses of the liver

Liver is a target organ of drugs and toxic chemicals. It is a target organ because of its large blood supply leading to pronounced toxicant exposure and accumulation; its clearance function involving microvasculature, hepatocytes and intrahepatic biliary system; and its pronounced metabolic capacity. The main functions of the liver, which are synthesis and redistribution of nutrients and intermediary metabolites, biotransformation, and bile formation, may be involved in the generation of hepatic

lesions.

Chemical injury to the liver is a many-faceted phenomenon. The diverse aspects include the nature of hepatotoxic agents, the type of injury, the mechanism for the hepatotoxic effects, and the circumstances of exposure. There are a variety of chemical agents that can induce hepatic injury. Some hepatotoxins found in nature are products of plant, fungal or bacterial metabolism or are minerals. Many hepatotoxic agents are products of the chemical or pharmaceutical industry. Still others are inductrial byproducts or waste materials that, by polluting the environment, may gain access to humans. Hepatotoxic injury can have several forms. Some agents lead to necrosis, steatosis, cirrhosis or carcinoma (Zimmerman, 1998). Others lead only to interference with bile secretion, with little overt injury to the hepatic parenchyma. Some produce curious degenerative or vascular lesions. The entire range of known hepatic lesions can be produced by drugs or other chemicals (Ishak and Zimmerman, 1995).

Current knowledge of hepatotoxicity is derived from several sources. Studies of the phenomenology of accidental toxic injury in humans have provided a clear picture of the clinical and histological effects of exposure to intrinsic hepatotoxins (e.g., carbon tetrachloride, chloroform, white phosphorus). Experimental studies have added depth to this information by analysis of structural, ultrastructural, and functional changes in the liver; description of the rate of evolution of lesions; elucidation of mechanisms of injury; and definitions of factors that affect vulnerability. Contributions of molecular biology, pharmacology, physiology and biochemistry have helped to unravel mechanisms for

injury by many of the hepatotoxins.

Repeated chronic injury will cause hepatic fibrosis. It is characterized by an excessive deposition of extracellular matrix (ECM) proteins, especially fibrillar collagens, including types I and III collagens (Bataller R, Brenner DA, 2005). Following chronic liver injury, inflammatory lymphocytes infiltrate the hepatic parenchyma. Some hepatocytes undergo apoptosis. Kupffer cells activate, releasing fibrogenic mediators, including cytokines such as transforming growth factor-β (TGF-β), platelet-derived growth factor (PDGF), and tumor necrosis factor-α (TNF-α) (Henderson N., Iredale P, 2007). The hepatic stellate cell (HSC) is the primary cell-type in the liver responsible for excess collagen synthesis during hepatic fibrosis. Following liver injury, the HSC undergoes a complex transformation or activation process where the cell changes from a quiescent, vitamin A-storing cell to that of an activated, myofibroblast-like cell. The pattern of gene expression changes following HSC activation; notably, a dramatic increase in TGF-β1, types I and III collagens occurs (Wu J, Zern M.A., 2000).

Many chemicals, such as carbon tetrachloride (CCl4), dimethyInitrosamine (DMN), and thioacetamide (TAA) have been used as model toxins to study hepatotoxicity or to produce liver disease model (e.g., fibrosis, carcinoma) in mammals (Fatima et al, 2006). In this project, TAA has been chosen to induce liver lesion in medaka fish, because it is soluble and stable in water. A single dose of the compound can produce centrilobular hepatic necrosis and that chronic administration led to cirrhosis and carcinoma (Zimmerman, 1999). TAA belongs to the category of indirect hepatotoxins, which cause

hepatic injury by producing selective biochemical or physiologic lesions that disrupt the metabolism or integrity of hepatocytes. In contrast, the direct hepatotoxins are agents that destroy hepatocytes. A metabolite of TAA, formed by action of the amine oxidase of Zeigler (flavoprotein monooxidase) rather than by P450-dependent enzyme systems, is responsible for the hepatic injury. TAA is converted to thioacetamide-S-oxide, which is presumably converted to an active toxic metabolite that binds covalently to tissue molecules, provoking necrosis.

1.4 Nonlinear microscopy for tissue imaging

The histological extent of liver damage has been estimated mainly by qualitative observation on the liver tissues after staining. These methods are based more on the alteration of architecture, cell density, nuclear shape, or distribution patterns of fibrosis. Thus the results rely heavily on the visual interpretation of the observer (Masseroli et al, 2000). Computerized image analysis has also been introduced into hepatic lesion assessment, wherein the images of properly stained liver slice are captured by a digital camera and the area of inflammatory cells (Hodgson et al, 2006), proliferating cells (Lake-Bakaar et al, 2002) or collagen (Dahab et al, 2004) in the images are calculated by software after image segmentation. However, this application of image analysis is limited due to the intrinsic characteristics of histological staining and image acquisition methods.

In the mean time, the development in mode-lock laser technique and weak optical signal detection has made nonlinear optical microscopy (multi-photon and excited fluorescence and multi-harmonic generation) an affordable technique for thick tissue imaging (So and

Kim, 1998). Besides the advantages shared by all nonlinear microscopies, e.g. deeper penetration depth, intrinsic optical sectioning, and less out of focus photobleaching and phototoxicity, second harmonic generation (SHG) is a non absorption process and no photochemical damage happens to specimens even in focal plane. It is sensitive to highly ordered structures without centrosymmetry. Collagen is known to induce SHG (Cox et al, 2003). Imaging of collagen in tumor demonstrated that SHG signal could readily image the highly fibrillar subpopulation of collagen I and did not image elastin, collagen IV or other basement membrane components (Brown et al, 2003). SHG signal is a narrow peak in spectrum and can be well separated from fluorescence by a narrow bandpass filter, resulting in clean images with extremely low background. These feature make SHG an excellent tool for quantitative assessment of liver fibrosis, as fibrosis is mainly characterized by excessive deposition of collagen type I. Simultaneously, two-photon excited fluorescence (TPEF) images of hepatocytes can be obtained from the same unstained tissue slices. The excited autofluorescence of hepatocytes comes from intrinsic molecules abundantly existed in hepatocytes plasma, such as NAD(P)H and flavins (Zipfel et al, 2003). Degenerated hepatocytes form dark regions in TPEF images. Thus, combining the TPEF and the SHG imaging, the information of pathological process of liver degeneration and fibrosis including subtle changes in hepatocyte morphology and collagen fibers can be easily obtained and quantified.

1.5 Aims of the project

The hypothesis this study based on is that medaka has similar pathological responses as mammals to injuries by hepatic toxins. Under this hypothesis, it is expected that

expression of molecular markers such as Collagen type I and TGF-β would increase upon repeated and chronic injury by TAA. Histological change is also expected in medaka liver due to cell necrosis, steatosis and collagen deposition. Thus medaka can be an alternative hepatotoxicity model to mammals, which is more cost-effective and statistically efficient.

This study first aimed at establishing a hepatotoxicity model using medaka fish by TAA treatment. Conventional methods, such as RT-PCR and H&E staining, were used to validate the model, by examining the mRNA expression of specific genes and the histological changes of the liver tissue. After establishing this model, nonlinear microscopy (TPEF/SHG) was developed and applied for liver tissue imaging, which requires no staining. Image processing algorithms were developed subsequently to quantify the degree of liver damage. At last, an RFP labeled liver was imaged under TPEF in three-dimensional manner. Study of image depth enhancement was carried out for future application of TPEF/SHG microscopy on whole organ imaging.

CHAPTER 2 MATERIALS AND METHODS

2.1 Animals

Medaka fish were obtained from Dr. Hong Yunhan's lab at the Department of Biological Sciences. Fishes were maintained in indoor aquarium at a temperature of 25^{o}C – 28^{o}C. Rectangular plastic containers with volume of 8 liters were used to culture the fish. A container of this size can hold about 40 adults. The fish were fed with nauplii of brine shrimp (Artemia salina) twice daily. Tap water that stood longer than two days was used to keep the fish. Tap water cannot be used immediately after it is drawn, because it is usually treated with chlorine and other chemical agents. Two extra containers filled with reservoir water were placed in the aquarium and used for changing water. This procedure was desirable for two reasons: first, the harmful effect of chlorine was avoided and second, the same temperature as that of fish containing aquaria was obtained. The photoperiod in the aquarium was 12 hours of light and 12 hours of dark.

2.2 Chemical Treatments

Specimens used in this study were approximately 3-months old, reproductively mature, regardless of the sex. Fish were incubated in TAA-containing water to induce liver damage. Thioacetamide (TAA) was purchased from Sigma-Aldrich (163678).

A preliminary study has been carried out to determine the concentration range of TAA. When TAA concentration was lower than 0.025%, the fish survival rate was not changed

as compared to normal fish after continuously 4 weeks' exposure. When TAA concentration was 1.2%, no fish left after 1 week's exposure. So in further studies, the TAA concentration was varied from 0.025% to 1.2%.

Two exposure protocols were designed to assess the short-term and long-term toxic effect of TAA. For acute liver damage, fish were treated with TAA for 14 hours every other day for 1-week. For chronic liver damage, fish were treated for 2 hours daily for 4-weeks. The fish treatment scheme was summarized in Table 2.1. There were 20 fish in each group, as limited by the volume of the container.

Table 2.1 Fish treatment scheme

Test group / Conditions	1	2	3	4	5	6
TAA conc.	0.05%	0.1%	0.2%	0.4%	0.8%	1.2%
Exposure time	2h/ 14h	2h/ 14h	2h/ 14h	2h/ 14h	2h/ 14h	2h/ 14h
Exposure freq.	Daily /every other day	Daily/ every other day	Daily/ every other day	Daily/ every other day	Daily/ every other day	Daily/ every other day
Treatment period	Until inducing liver fibrosis as diagnosed by RT-PCR and histology.					
Age of fish	Reproductively mature, the same batch					
Dilution water	Dechlorinated tap water					
Water temperature	24±2°C					
Photoperiod	12h light, 12h dark					
Solution volume	2L. Change solution every week					
No. of fish	20 per group					
Feeding regime	*Artemia* nauplii twice daily when fish are in normal water					
Endpoints	Survival, histology, RT-PCR					

The target fish were kept in two-liter rectangular containers with mesh in the bottom (Figure 2.1). The mesh containers were then put in the bigger containers (8L) with dechlorinated tap water inside (Figure 2.2). When there is no treatment, the fish were cultured and received food in normal conditions. During TAA treatment, the mesh containers, together with the fish, were moved from normal water to the TAA containing

water (Figure 2.3). TAA containing water was kept in sealed plastic containers when there is no treatment (Figure 2.4), and the solution was changed every week. After certain period of time (2h or 14h), the mesh container and fish were taken out and washed in dechlorinated tap water for two times, and moved back to the normal water.

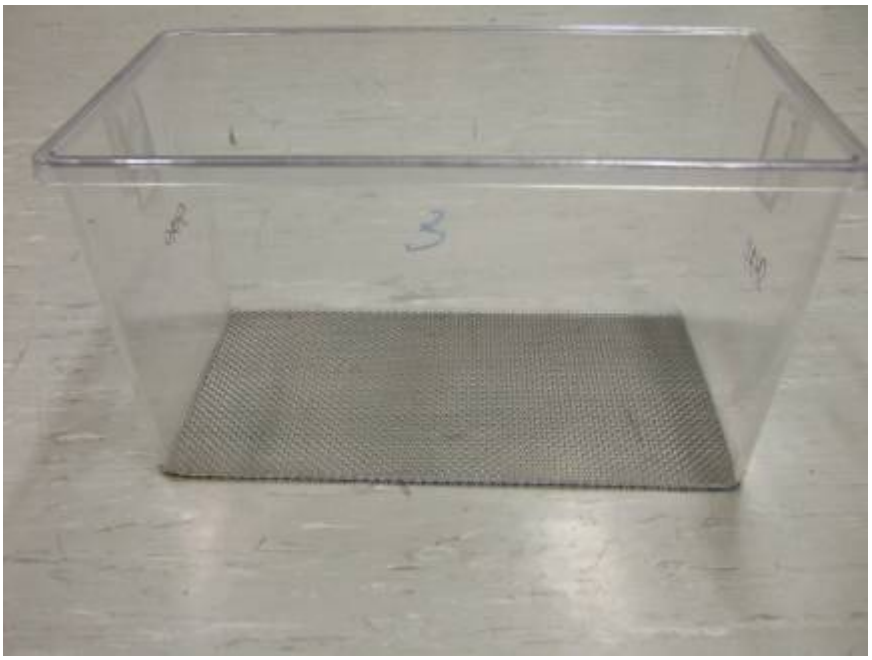

Figure 2.1 Two-liter rectangular container with mesh bottom.

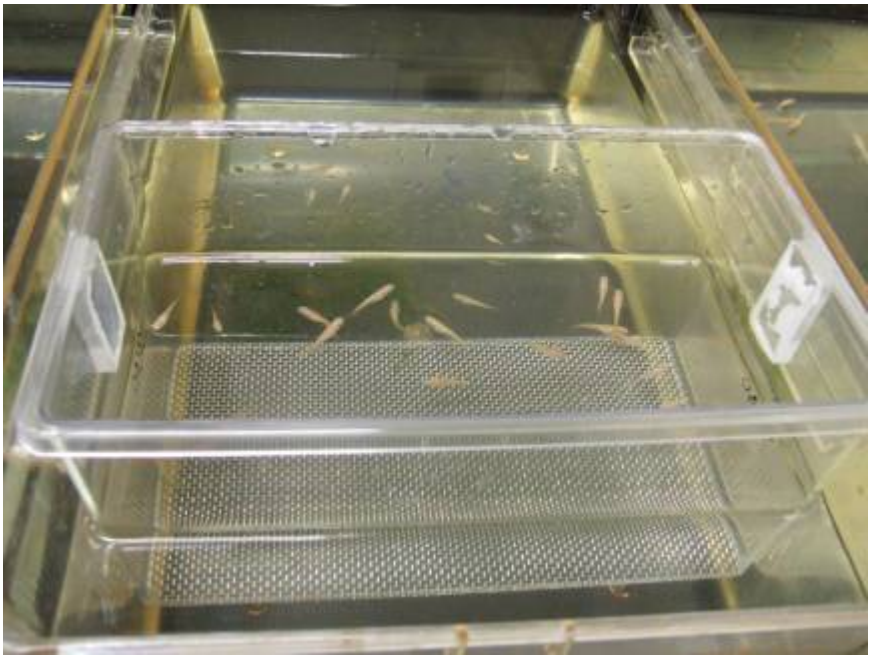

Figure 2.2 Fish together with mesh container inside the eight-liter tank.

Figure 2.3 Fish together with mesh container inside TAA containing plastic container.

Figure 2.4 Sealed plastic container with TAA solution inside.

2.3 RNA isolation

For RNA isolation, adult medaka fish were placed in ice-cold water for 2 min to anesthetize and kill the fish. Its surface was sterilized by spraying and swapping with 70% ethanol. Surgical tools were sterilized by autoclave. Adult medaka male and female fishes were distinguished by their urinogenital papilla, anal and dorsal fin (http://biol1.bio.nagoya-u.ac.jp:8000/medaka's.jpeg). According to the fish anatomy (http://www.infovisual.info/02/033_en.html), the fish were dissected laterally. Livers were extracted and collected separately into 1.5-ml RNases-free Eppendorf tubes for total RNA extraction immediately.

Total RNA was extracted from the whole liver of adult medaka using the Trizol reagent (Invitrogen, Life Technologies, USA). Each liver tissue (approximately 10 mg) was homogenized independently in 0.8 ml Trizol reagent by RNases-free Micropestle (Eppendorf). 0.16 ml of chloroform was then added and sample vortexed, followed by incubation at RT for 3 min. The samples were then centrifuged at 12,000 rpm for 15 min at 4°C. The aqueous phases contained RNA and were transferred to a fresh RNases-free tube. RNA was precipitated by the addition of 0.4 ml of isopropyl alcohol, incubated at room temperature for 10 min and pelleted down by centrifuging at 12,000 rpm for 10 min at 4°C. Total RNA pellets were then washed twice with 1 ml of 75% ethanol (in 0.1% DEPC-treated water), centrifuged at 7,500 rpm for 5 min at 4°C. Finally, the RNA pellets were resuspended in 30 µl to 60 µl of 0.1% DEPC-treated water and incubated at 60°C for 10 min, before storing at -80°C.

RNA concentration was determined by OD_{260} measurement. 4 µl of diluted RNA was added to a cuvette containing 800 µl of DEPC water. Then OD_{260} value were read and recorded. Finally, RNA concentration = OD_{260} x 200 (dilution factor) x 40 (factor for RNA) µg/ml.

2.4 cDNA synthesis

The first-strand cDNA was synthesized using Transcriptor First Strand cDNA Synthesis Kit (Roche). First, in a sterile, nuclease –free, thin-walled PCR tube, 1 µg of total RNA, 1 µl of anchored oligo-dT, and PCR-grade water were added to make total volume of 13 µl. The mixture was heated for 10min at 65^{o}C in a thermal block cycler with a heated lid, and immediately cooled on ice. After that, 4 µl of 5x Reaction Buffer, 2 µl of dNTP Mix (10 mM each), 0.5 µl of RNase Inhibitor and 0.5 µl of Transcriptor Reverse Transcriptase were added to the mixture. The final mixture was incubated at 55 ^{o}C for 30 min, followed by heat inactivation at 85^{o}C for 5 min. At last, 0.5 µl of RNase was added and heated at 37^{o}C for 20 min. The synthesized cDNA was then ready for PCR or Real-time PCR.

2.5 PCR and Real-time PCR

Polymerase chain reaction (PCR) is an *in vitro* method for enzymatic amplification of specific DNA sequences from minute quantities of DNA or RNA samples, using two oligonucleotide primers that anneal to opposite strands, flanking the region of interest in the DNA template. Cycles involving template denaturation, primer annealing, and extension of the annealed primers by heat-stable Taq DNA polymerase result in the exponential accumulation of a specific fragment whose termini are defined by the 5’ ends

of primers. PCR was performed on an Eppendorf Mastercycler System. Each reaction of 50 µl total volume in a thin-wall PCR tube contained 5 µl 10x polymerase buffer ($MgCl_2$ free), 4 µl of primers mix (10 µM each), 1 µl of NTP (10 mM each), 100 ng of template, 0.5 µl of *Taq* DNA polymerase (Promega) and PCR-grade water. The sample was denatured for 5 min at 94°C, followed by 30cycles. Each cycle consisted of 45s denaturation at 94°C, 45 min annealing at 55-60°C, and 1 min extension at 72°C, with a final 7-min extension at 72°C. The final PCR products were separated and analyzed on 1.5% agarose gels.

While traditional PCR uses agarose gels for the detection of PCR amplification at the final phase or end-point of the PCR reaction, Real-Time PCR allows for the detection of PCR amplification during the early (exponential) phases of the reaction, which is more sensitive and precise. Real-Time PCR is more suitable and useful for quantitative analysis.

Real-time PCR was carried out on a LightCycler (Roche Diagnostics) in 10 µL reaction. The reaction mixture contained 2.5 µL of sample (0.1-5 ng/µL), 1 µL of primers mix (3-5 µM), 2 µL of Sybr green taq ready mix (Roche) and 4.5 µL PCR-grade water. The concentration and annealing temperature of primers were optimized as described in Section 2.6. The standard curve was plotted by β-actin amplification. Basically, cDNA samples synthesized in Section 2.4 were diluted by 1:10, 1:50, 1:100 and 1:500. Four reactions containing each of the diluted samples were carried out simultaneously. A cycle number was obtained for each sample. Then the standard curve was obtained by plotting

the cycle numbers v.s. log of theoretical sample concentrations. One of the diluted samples was chosen as template for diagnostic analysis of other genes, based on their cycle numbers, i.e., the original concentration of cDNA. For quantitative analysis of a specific mRNA content, concentration was first calculated from the standard curve using cycle number. Then a relative value was obtained from the ratio of the concentration of the specific mRNA and β-actin. This relative value was used for quantitative analysis of the mRNA content in different tissue samples.

2.6 Primer design and optimization

The quality of primers is very crucial in Real-time PCR because of its high sensitivity. Design of primers for Real-time PCR is much stricter than for traditional PCR. Primers were designed using OLIGO 6. The primer length should be between 16-21 bp and product length between 200-500 bp. GC (or AT) content should be between 40-60%. The primer sequences were elected manually to make sure that self-dimers and upper-lower dimmer were less than 2 bp and no hairpin stem was formed.

The concentration and annealing temperature of primers for Real-time PCR need to be optimized so that no dimer produced when there was no template added. The primer optimization started with the initial annealing temperature calculated by OLIGO 6 and concentration of 5 μM. If dimer appeared in control reaction (Figure 2.5a), annealing temperature should be increased by 1-2 °C, or concentration reduced to 3 μM, or both, until no dimer produced in control reaction (Figure 2.5b). If these adjustments can not work, the primer should be redesigned. The sequences and conditions of primers used in

this project were listed in Table 2.2.

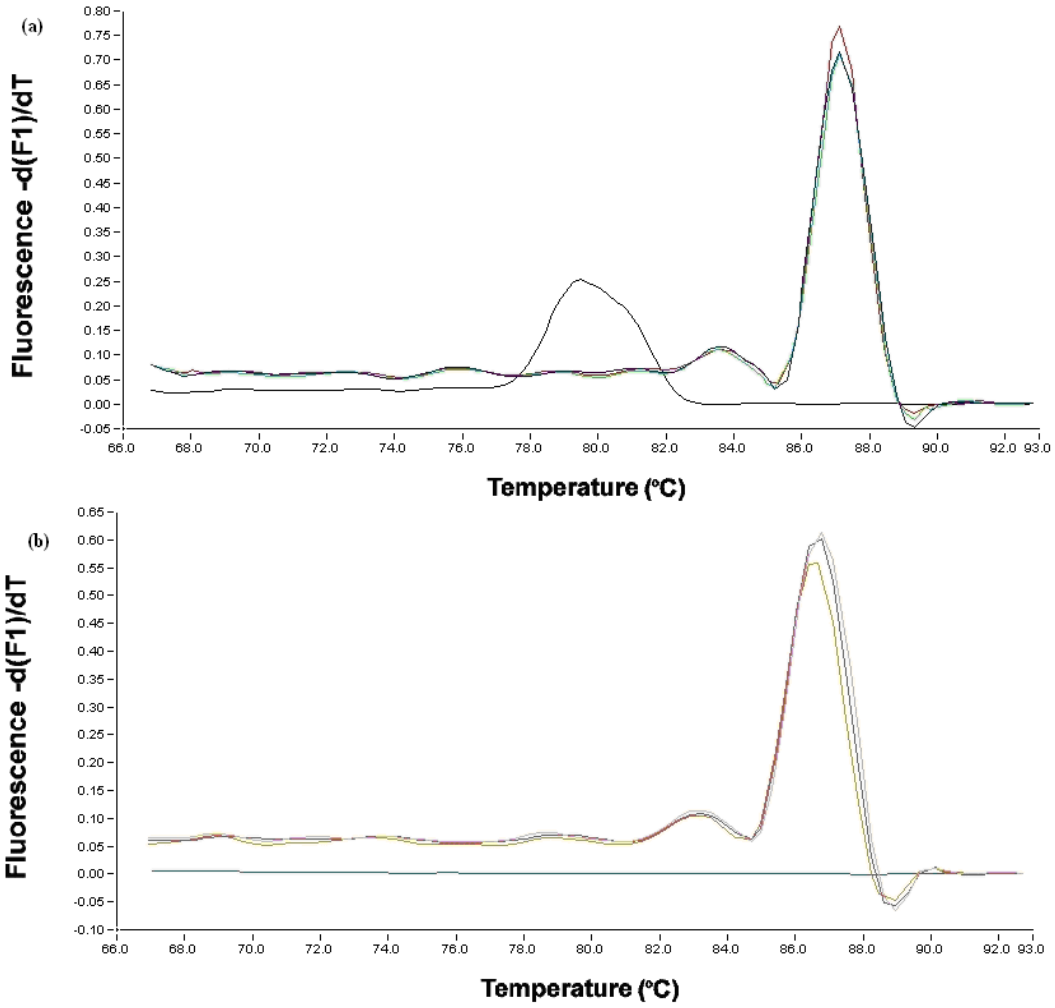

Figure 2.5 Melting curve of Real-time PCR. a) Dimer formed in control reaction (no template added). b) No dimer formed in control reaction. The melting curve is a flat line.

Table 2.2 List of primers for Real-time PCR.

Gene	Primer sequence	Product length (BP)	Annealing temp. (°C)	Conc. (μM)
β-actin	Sense 5'-CTTCCTTCCTTGGTATGG-3' Antisense5'-TGTGTGGTGTGGTTTTGA-3'	403	55	5
Col1	Sense 5'-GTTCCGTGCTGATGATGC-3' Antisense5'-CGTGCTTCTTCTCCTTGAT-3'	326	57	5
TGF-β1	Sense 5'-TGCGTGTTTTCTGCGATT-3' Antisense 5'-GTCTCCGTTTGGGCTGTA-3'	220	56	5

2.7 Tissue preparation

Tissues were prepared carefully to keep good morphology for histology and imaging, since medaka liver is so tiny and fragile. After euthanasia by ice shock, the head was cut off from the spinal cord. Then the right abdomen was opened without perturbing the liver tissue. Before isolating the liver, the whole fish bodies were fixed in 4% paraformaldehyde/PBS for 4 hours. Then liver were easily separated from the fixed bodies and re-fixed in 4% paraformaldehyde/PBS overnight at 4 °C.

For histological staining, the fixed liver were then processed to paraffin blocks by the following procedures: 30 min 70% ethanol, 30 min 80% ethanol, 45 min 95% ethanol, 45 min 95% ethanol, 1 h 100% ethanol, 1 h 100% ethanol, 30 min xylene I, 30 min xylene II, 30 min xylene III, 2 h wax I, 2 h wax II and 2 h wax III. The paraffin blocks were cut into 4μm thick sections and dried at 42 °C hot plate overnight. For deparaffinization, slides were washed in 2 changes of xylene for 3 min each. Slides were then transferred to 100% ethanol after blotting excess xylene. The sections were cleared by 100% ethanol, 95% ethanol and 70% ethanol, for 3 min each. Cleared slides were washed in deionized water for 5 min. Then the slides were ready for histological staining.

For TPEF/SHG imaging, the sample preparation was much easier. The fixed liver samples were immersed in 20% sucrose/PBS overnight or until it sank to bottom. The cryoprotected samples were then transferred to embedding mold, filled with 20% sucrose: Tissue-Tek optical cutting temperature compound (O.C.T.), and let stand for 4 hours at room temperature. Then the samples were frozen in -80 °C freezer. The frozen tissue

blocks were cut into 30 thick sections and stored at -80 °C until needed. Before TPEF/SHG imaging, slides were removed from freezer and allowed warming to room temperature and air dried. O.C.T. was washed away by 2 changes of 100% ethanol for 1 min each. Then the liver sections were ready for imaging.

2.8 Histology

For Hematoxylin and Eosin (H&E) staining, slides were first stained in Harris's Hematoxylin for 2 min after deparaffinization, and rinsed with tap water for 5 min. Then they were dipped in 1% Acid Alcohol (1 ml HCl in 100 ml 70% ethanol) for 1 s and rinsed with water. Then they were dipped in Alkaline solution (2 ml 0.2% Ammonium hydroxide in 1L water) for a few seconds to 'blue' the sections, and rinsed in water. After that slides were stained in Eosin for 3 min and rinsed in water. Then they were dehydrated by the following procedures: 70% ethanol for 20s, 95% ethanol for 20s and 100% ethanol for 3 min. Finally they were cleared in 2 changes of xylene for 7 min each, and mounted by DePex mounting medium. H&E staining stains nuclei blue-black and cytoplasm pink. It was used to look at the morphological change of damaged liver.

For Sirius red staining, deparaffinized slides were stained with Harris's haematoxylin for 2 min and washed under running tap water for 5 min. The slides were then stained in picro-sirius red for one hour. Picro-sirius red solution was prepared by dissolving 0.5g Direct Red 80 (Fluka) in 500 ml saturated aqueous picric acid solution. Then the slides were washed in three changes of acidified water (5 ml acetic acid in 1 L of distilled water). After removing most of water from the slides by vigorous shaking, the slides were

dehydrated in three changes of 100% ethanol, cleared in 2 changes of xylene and mounted by Depex mounting medium. Sirius red staining is a useful technique for collagen visualization in liver biopsies. It stains collagen bright red and hepatocytes dull yellow. In this study, it was used to qualitatively examine the collagen deposition in damaged liver.

2.9 Nonlinear optical microscopy

The nonlinear optical microscope is modified on a Carl Zeiss LSM 510. Figure 2.6 illustrates the optical configuration schematically. The excitation source is a mode-lock Ti: Sapphire laser (Mai-Tai broadband, Spectra-Physics) with a pulse width of no more than 100fs and repetition rate of 80MHz within the tunable range 710-990nm. After attenuated by a computer controlled acousto-optic modulator (AOM), the laser beam is delivered into the XY scanner, and then reflected into an objective by a piece of short pass filter. The laser is then focused to a spot on the specimen, where nonlinear optical processes occur. TPEF is distributed in 4π solid angle and collected by the same objective. After removing the back scattered laser by the short pass filter, the signal is directed to detection system, where two channels with different wavelengths can be detected simultaneously. Due to the intrinsic optical sectioning capability of nonlinear optical process, there is no pinhole needed in the optical path. In contrast with TPEF, SHG signal is mainly distributed in the forward direction and collected by a condenser with a numerical aperture larger than that of the objective. After filtering out the fundamental harmonic by a short pass filter, the optical signal is deflected to either a photomultiplier tube (PMT) or spectrometer by a flop mirror. In order to record clean SHG signal, TPEF

collected by the condenser is removed by a band pass filter before the PMT. In the spectroscopy path, the signal is couple into an optical fiber bundle and delivered to the entrance slit of the spectrometer (Acton Research SP2300i). After dispersed with a 1200g/mm grating, a spectrum is recorded by a thermoelectrically cooled charge coupled device (SPEC-10, Princeton Instruments). The PMTs used in this system are Hamamatsu R6357, which is a meshless multialkli compact model with the mesh removed.

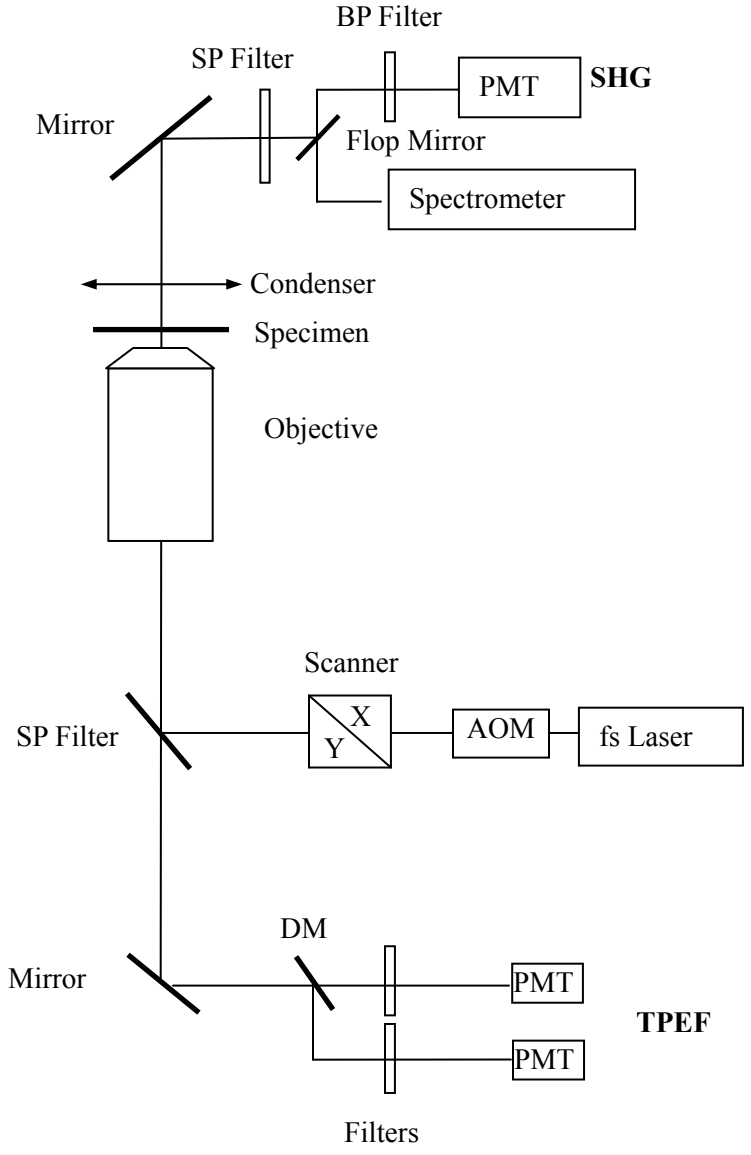

Figure 2.6 Schematic of TPEF/SHG microscopy.

2.10 Image acquisition procedures

For histologically stained liver slices, images were taken by an inverted microscope (CKX-41, Olympus). The transmission bright field images were captured by a 5M-pixel camera (MicroPublisher 5.0 RTV QImaging). Objectives of 10x (N.A. 0.45) and 40x (N.A. 0.75, oil immersed) were used.

For TPEF/SHG imaging, the cryosectioned slices dehydrated and air dried were mounted with distilled water rather than normal fluorescence mounting medium, without histological or immunofluorescence staining. The slides were imaged under TPEF/SHG microscopy before mounting water evaporated.

The microscope was controlled by Zeiss LSM imaging software. All optical components (e.g. objectives, filters, beam splitters) and parameters (e.g. wavelength, spatial resolution, and pinhole size) can be adjusted through the software. TPEF and SHG signals were obtained simultaneously under excitation wavelength of 900 nm. A beam splitter of KP650 (short pass 650 nm) was used to reflect the excitation laser to objective. TPEF imaging collected the autofluorescence signal of hepatocytes using reflected mode. A filter of KP685 (short pass 685 nm) was used to filter out unwanted signals that have wavelength longer than 685 nm. No pinhole was needed in TPEF imaging so the pinhole size was set to be maximum to obtain signal as much as possible. SHG imaging collected the second harmonic generation signal of collagen type I and is more effective in the transmission mode. A band pass filter of 450nm was placed in the transmission pathway to collect the pure SHG signal.

The objectives used to obtain images were 10x or 20x. Images were 12-bit and 1024x1024 in size. The spatial resolutions were 0.9 μm for 10x objective and 0.45 μm for 20x objectives. To obtain a picture of the whole liver section, tiles can was used to construct large images. Tile scan was controlled by the computer. Upon completion of each single image, the specimen was translationally shifted one image size by a motorized stage. The number and center of tile scan images can be defined by the software. Finally a matrix of images was stitched to form a large image. For a typical fish liver section, the whole image can be obtained by a 4x4 image matrix for 10x objective or 8x8 matrix for 20x objective.

2.11 Quantitative analysis of liver damage

TPEF/SHG images were taken from unstained liver slices and contained little artifact. The signal to noise ratio was also higher than images taken by light microscopy. Thus TPEF/SHG images were very suitable for quantitative analysis. TPEF and SHG images were taken separately by two PMTs and can be analyzed independently. SHG signal originated from collagen type I and can be used for quantification of liver fibrosis. TPEF signal originated from hepatocytes and can be used for quantification of cell necrosis.

For quantification of collagen content, SHG signals were separated from the background by segmentation, to eliminate the influence of noise and background. For simplicity in implementation, threshold segmentation was adopted. Otsu method (Otsu, N., 1979) was used to optimize the threshold for each image. The method is outlined here. For each threshold t, an image is split into two groups (object and background) based on pixel

intensity. The weighted sum of intragroup variances, σ_w^2, is calculated as follow,

$$\sigma_w^2(t) = q_1(t)\sigma_1^2(t) + q_2(t)\sigma_2^2(t),$$

where $q_1(t) = \sum_{i=0}^{t-1} p(i)$, $q_2(t) = \sum_{i=t}^{N} p(i)$, $p(i)$ is the probability of the histogram at grey scale i and N is total number of grey scale. $\sigma_1^2(t)$ is the variance of pixel intensity in the first group ($< t$,background), $\sigma_2^2(t)$ is the variance of the pixels in the second group ($\geq t$, object). Then σ_w^2 is computed for all possible values of t, the t producing the minimum σ_w^2 is the optimal threshold T. The algorithm is implemented through Matlab R14 (The Math Works, Inc, Natick). Since the threshold segmentation method used here processes each pixel independently, grainy noise will affect segmentation. In order to remove the isolated pixel noise and join separated portions of features in the binary images generated by the segmentation, erosion followed by dilation operation were applied to improve the accuracy of quantification (Serra, J., 1982).

In histological staining method, pixel intensity is influenced by sample preparation and image acquisition, therefore image area is used to characterize collagen. In SHG microscopy, signal intensity is determined by laser power and numerical aperture of the collection optics rather than sample preparation. Thus the signal is highly reproducible in SHG. During fibrosis, the increase of collagen in the lateral directions is measured in area while the depth dimension is reflected in signal intensity. Therefore, changes in total signal intensity resemble the collagen variation more closely and thus were adopted in this work. In addition, total intensity can tolerate the error in segmentation because

ambiguity always occurs in low intensity regions (object boundary). Wrong classification of dim pixels will affect total intensity less than total area. However, if the summation was done over the whole image, the background level and noise would affect the result greatly. To rule out the deleterious effect, the segmented image was used as a mask to screen out the background in the original image. It is implemented by multiplying the original image with the mask image pixel by pixel. Only the intensity of collagen signal was counted. The total intensity was then normalized to the whole area of the image to make the quantities comparable for different experiments.

During hepatotoxin induction, some hepatocytes were degenerated and formed dark regions in TPEF images. To quantitatively describe this process, the TPEF images were first subjected to a low pass filter to suppress noise. Threshold segmentation was applied subsequently, followed by erosion and dilation to remove the small dots and connect broken features. Then the area and aspect ratio of each object in the processed images were calculated and objects were classified according to these two parameters. Sinusoidal spaces appear generally narrow strips in TPEF images, possessing high aspect ratios. However, aspect ratio itself cannot be used to identify sinusoids because a string of necrotic hepatocytes also appear long patches. To distinguish them, object area normalized to aspect ratio is used as a criterion. If the normalized area is smaller than a critical value (normalized area of single hepatocyte was chosen in this work), this object was considered as sinusoidal space and not counted in cell necrosis analysis. Blood vessels were also excluded in total necrosis area calculation, which was recognized by the large area and shape.

CHAPTER 3 RESULTS

3.1 Histological study of medaka liver anatomy

An understanding of chemical hepatotoxicity requires an appreciation of anatomic and physiologic features of the liver. With respect to fish liver, it is important to emphasize that although fish and rodent livers are similar in many features, there are many differences that may strongly influence chemical toxicity. We have studied the anatomic feature of medaka liver, which is similar to most of the teleost fish and different from mammals in many features.

The anatomic feature of medaka fish liver was studied by H&E staining. The whole fish was fixed and embedded into paraffin block. So the architecture of liver was well preserved and not distorted by outside force. Figure 3.1 shows one of the transverse sections from the middle of the organ. It also indicated the actual size of a medaka fish liver, around 3mm x 3mm x 2mm. Like most teleost fish, certain features of the hepatic gross and microscopic anatomy of medaka fish are different from those of mammalian liver. First, gross inspection of medaka livers reveals the form of a single lobe, whereas livers of mammals have multiple lobes. Second, the classic lobule structure of mammalian liver, which includes a central vein and portal tracts at the corner, is not present in livers of medaka fish (Figure 3.1). The stromal elements are spatially organized as venous-biliary-arteriolar tracts (VBAT), venous-arteriolar tracts (VAT), biliary-arteriolar tracts (BAT), venous-biliary tracts (VBT), biliary tracts (BT), arteriolar tracts (AT), and isolated veins (Rocha et al, 1995). These components are not two- but

three-dimensional entities, only serial sectioning allows a definite recognition of them. Few isolated veins at the transverse and longitudinal direction were observed in Figure 3.1. Figure 3.2 and Figure 3.3 show a higher magnification of vein and biliary-arteriolar tract, respectively. The VBAT, VAT, and VBT are considered portal tracts; the adjacent parenchymal zones are viewed as periportal areas. The veins emerging from those tracts are regarded as afferent, and related with periportal zones. The isolated veins are viewed as efferent.

Third, hepatocytes are typically arranged into cords with one hepatocyte thick and separated by sinusoids in mammalian liver. In medaka liver, a double row of hepatocytes arranged into tubules. Because there is no central vein and portal tract, and the veins, arterioles and biliary tract arrange in 3-dimmential manner, the hepatocytes and sinusoids also arrange in 3D. In Figure 3.3, hepatocytes and sinusoids appear to be in mosaic pattern that transverse and longitudinal sinusoids interleave rows or columns of hepatocytes.

Figure 3.1 Transverse section of whole medaka liver. The classic lobule structure of mammalian liver, which includes a central vein and portal tracts at the corner, is not present.

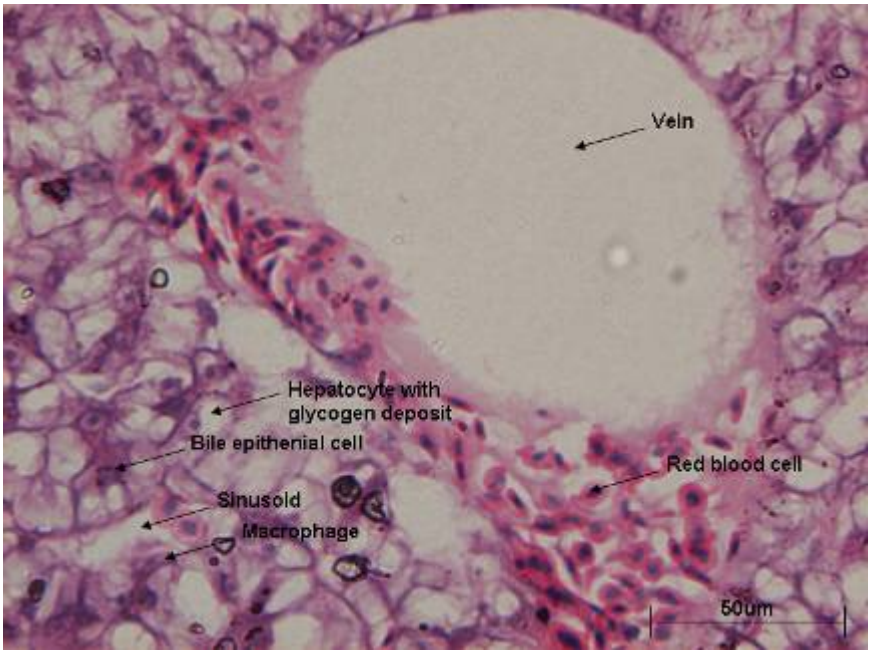

Figure 3.2 Higher magnification view of the vein of medaka liver showing an isolated vein.

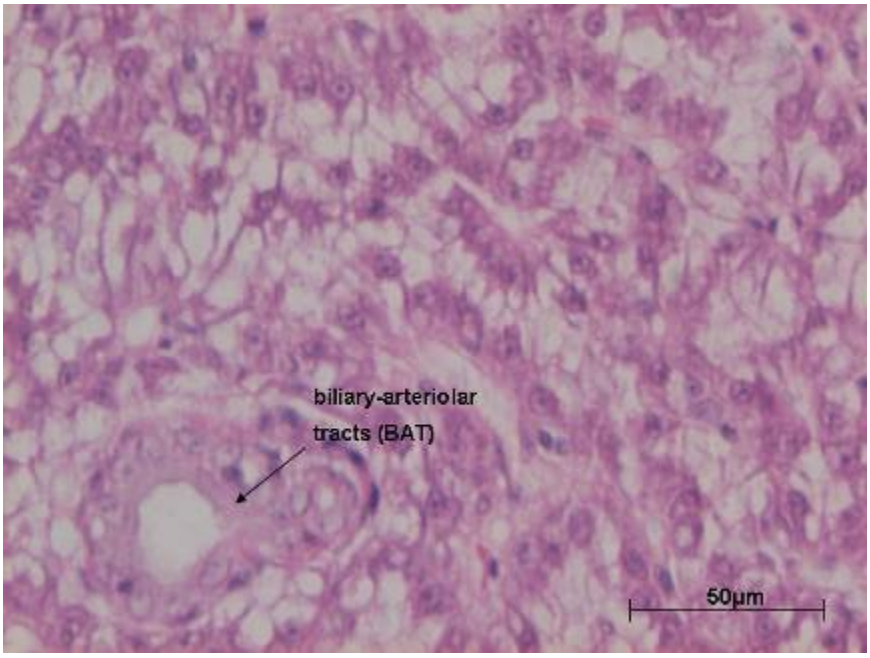

Figure 3.3 Higher magnification view of medaka liver showing biliary-arteriolar tract.

3.2 Chemical induction of liver damage

Thioacetamide (TAA) is a hepatotoxin that has been well studied in mammals. Administration of TAA by gastric incubation or by subcutaneous, intramuscular, intravenous, intraperitoneal, or intraportal administration produces zonal hepatic necrosis, renal tubular necrosis, and thymic injury. The LD_{50} dose for rats is approximately 200 mg/kg. Smaller single doses can produce necrosis, and with repeated administration, cirrhosis and hepatic carcinoma.

To examine the toxic response of medaka liver, TAA was administrated by water incubation. Adult fish absorb TAA molecules orally from the tank water (Langheinrich, 2003). There is no prior information on the lethal dose of TAA solution for fish. So we treated the fish with a series of TAA concentration, ranging from 0.05% and 1.2%, to find out the effective dosage on fish. The survival rates of medaka fish were recorded

daily under each condition. Under each TAA concentration, two treatment strategies were also designed to study the chronic and acute effect of TAA injury.

For chronic liver damage, TAA was administrated for 2 hours daily. The treatment was designed in such a way that the fish would receive repeated but not lethal injury and yet have time for recovery. This damage and repair process resembles the cause of liver fibrosis in human, which is the wound healing response to chronic liver injury. The concentrations we have used were 0.05%, 0.1%, 0.2%, 0.4%, 0.6%, 0.8%, and 1.2%. There are twenty fishes in each group. The survival rates at day 1, day 7, day 14 and day 28 were plotted in Figure 3.4. For TAA concentration of 0.2% and 0.4%, 3 independent experiments were carried out and mean survival rates were plotted with error bar representing standard deviation. From Figure 3.4, we can see that for TAA concentration higher than 0.4%, half of the fish died after 14 days; the survival rates were close to normal for TAA concentration lower than 0.4%. So 0.4% was considered the most effective TAA concentration for chronic liver damage. Lower concentrations caused little injury to fish, whereas higher concentrations were too toxic that fish were killed before the liver was chronically damaged.

For acute liver damage, TAA was administrated for 14 hours every two days. We considered this treatment as acute damage because the prolonged treatment time can be lethal and cause severe damage within short period of time (1 week). The concentrations we used were 0.05%, 0.1%, 0.2%, 0.4%. There are twenty fishes in each group. The survival rates at day 1, day 3, day 5 and day 7 were plotted in Figure 3.5. For the TAA

concentration of 0.2%, 3 independent experiments were carried out and mean survival rates were plotted with error bar representing standard deviation. From Figure 3.5, we can see that for the TAA concentration higher than 0.2%, half of the fish died after 5 days; the viabilities were close to normal for TAA concentration lower than 0.2%. So 0.2% was selected as the threshold of TAA concentration for acute liver damage. Lower concentrations were not effective to cause acute liver damage.

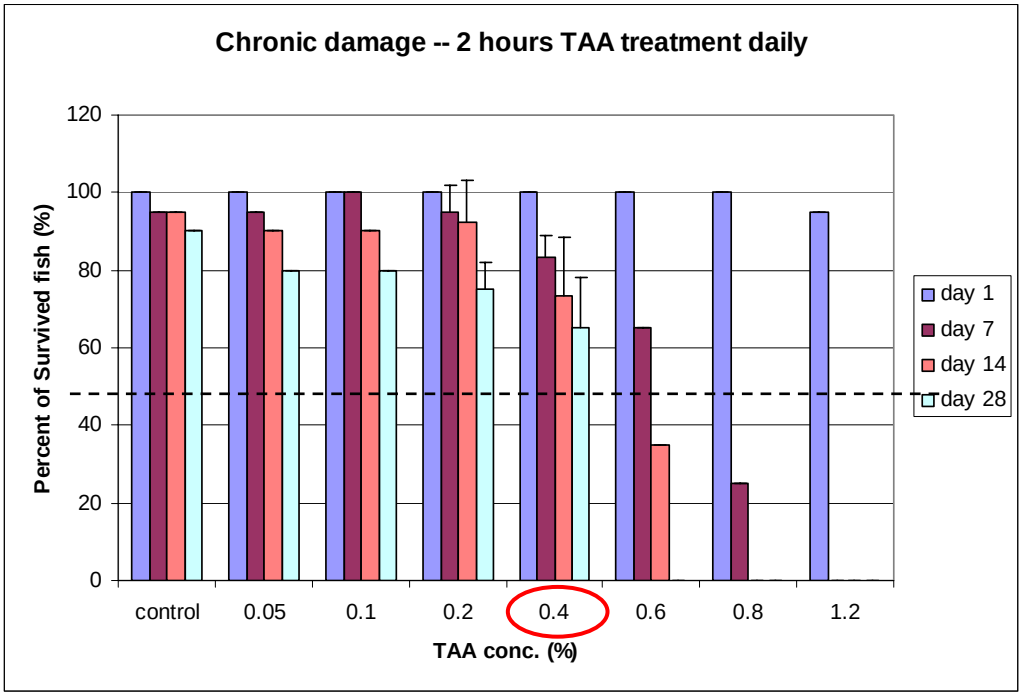

Figure 3.4 Survival rates of medaka fish after chronic TAA treatment. For the TAA concentration higher than 0.4%, half of the fish died after 14 days. 0.4% was considered as the most effective TAA concentration for chronic liver damage.

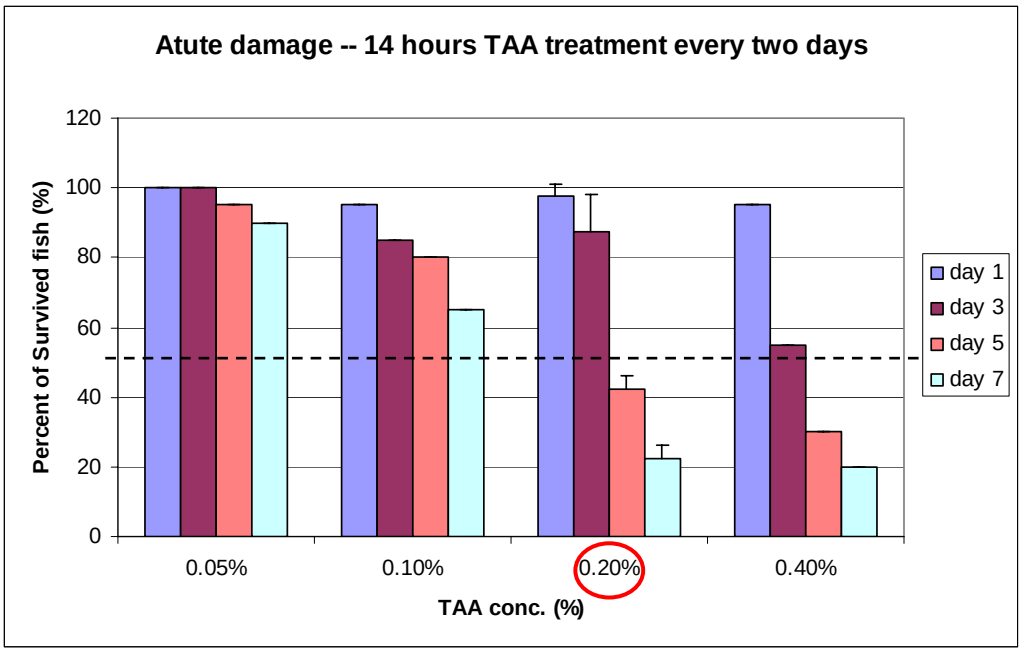

Figure 3.5 Survival rates of medaka fish after acute TAA treatment. For the TAA concentration higher than 0.2%, half of the fish died after 5 days. 0.2% was considered as the threshold of TAA concentration for acute liver damage.

3.3 mRNA expression of Procollagen I and TGF-β1

Procollagen type I and TGF-β are among the most important markers of liver fibrosis. Liver fibrosis is a wound healing process that occurs when the liver is injured chronically. The characteristic feature of liver fibrosis is an excess production of ECM, mainly type I collagen. TGF-β is an important cytokine in the regulation of the production, degradation, and accumulation of ECM proteins. High levels of TGF-β1 have been described in different acute and chronic liver diseases (Schnur J, et al., 2004). In order to assess the occurrence of fibrosis, we have examined the mRNA expression level of Procollagen type I and TGF-β1 in chronically TAA treated fish model.

The experimental design was shown in Figure 3.6. One group was control fish that reared in dechlorinated tap water. The other groups of fish were treated by 0.05%, 0.1%, 0.2%

and 0.4% TAA for 2 hours daily. At day 14 and day 28, three fish from each group were sacrificed. Liver samples were collected individually for RNA isolation and subsequent RT-PCR analysis.

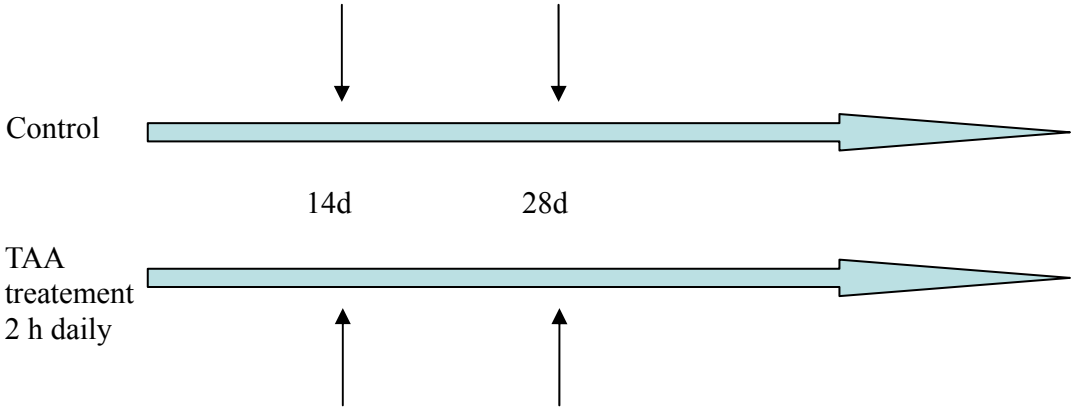

Figure 3.6 Experimental design of chronic liver injury. Fish were sacrificed at day 14 and day 28 from each group.

The Real-Time PCR results for Procollagen type I and TGF-β1 were plotted in Figure 3.7 and Figure 3.8 respectively. The mRNA expression levels were quantified by their relative value to β-actin. Remarkable increases in the expression level of the two important markers were detected in the 0.4% TAA treated group at 14 days. This observation reveals that 0.4% of TAA is effective for chronic liver damage in medaka fish, and liver fibrosis occurred at 14 days of o.4% TAA treatment. There was no up-regulation of Procollagen type I and TGF-β1 at 28 days, probably due to liver degeneration after long time of continuous injury.

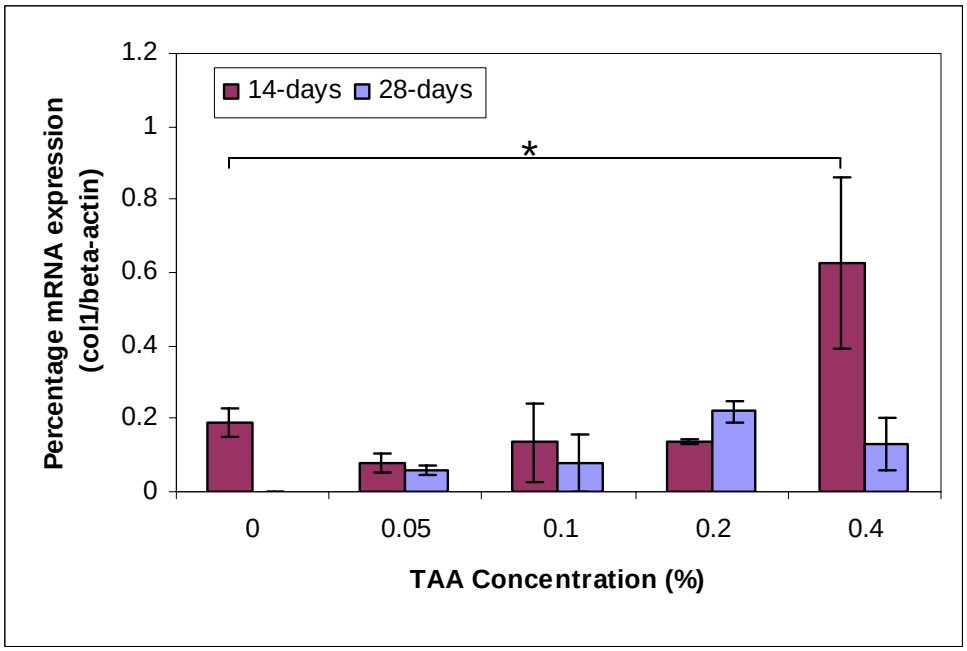

Figure 3.7 Percentage expression of Procollagen I relative to β-actin in control, 0.05%, 0.1%, 0.2% and 0.4% TAA treated fish liver. Remarkable increases in the expression level were detected in the 0.4% TAA treated group at 14 days. *: P<0.05.

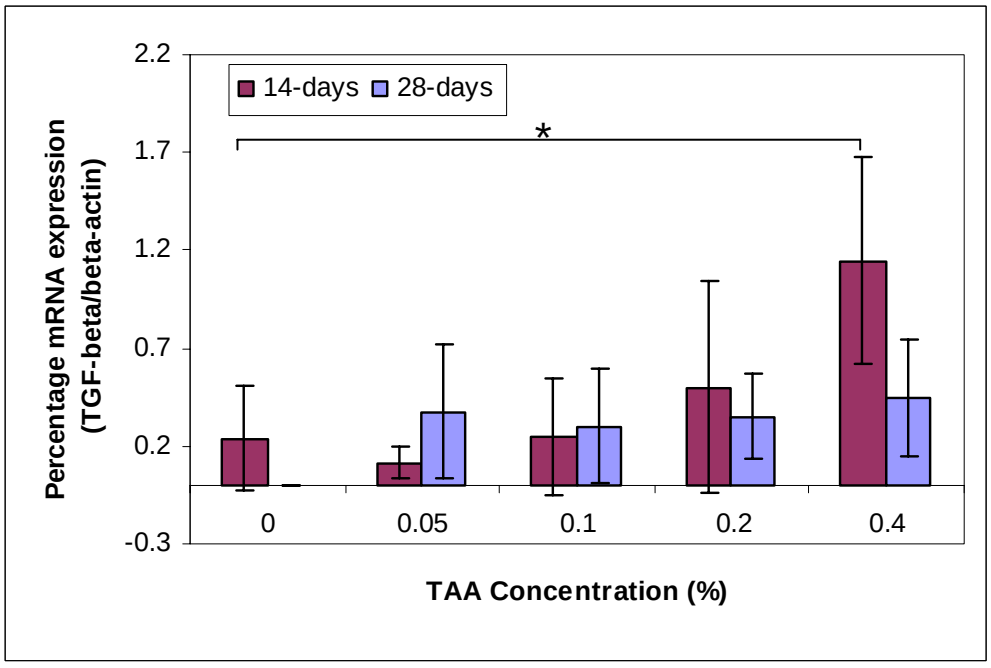

Figure 3.8 Percentage expression of TGF-β1 relative to β-actin in control, 0.05%, 0.1%, 0.2% and 0.4% TAA treated fish liver. Remarkable increases in the expression level were detected in the 0.4% TAA treated group at 14 days. *: P<0.05.

3.4 Histological assessment of liver damage

Liver damage was assessed by H&E staining and Sirius red staining. H&E stains nuclei and cytoplasm and reveals the cellular structure of liver tissue. Sirius red stains fibrous collagen and can be used to examines ECM deposition in damaged liver. Many microscopic changes, including inflammation, spongiosis, tumorigenesis, necrosis and fibrosis, were observed in chronically and acutely TAA treated medaka liver.

We have examined the liver sections of medaka fish 14 days after 2 hours daily exposure to 0.4% TAA. As compared to normal liver sections in Figure 3.1, 3.2 and 3.3, Figure 3.9, Figure 3.10 and Figure 3.11 show H&E stained liver sections revealing inflammation, spongiosis and tumorigenesis, respectively. Figure 3.9 shows a region of inflammatory cells around the hepatic vein and bile duct. Cell death evokes an inflammatory response which is manifested by the appearance of inflammatory cells. The majority of these inflammatory cells are lymphocytes (Orifei, 2003). The lymphocyte cells are generally smaller, with the cell nuclei smaller and darker than those of hepatocytes. Figure 3.10 shows spongiosis hepatis in the liver of a medaka fish. Spongiosis hepatis consists of multilocular cyst-like structures containing granular or flocculent eosinophilic material and occasionally erythrocytes. It is believed to represent a degenerative change in Ito cells and may be seen in normal hepatic parenchyma as well as in proliferative hepatocellular lesions such as foci and neoplasms. Figure 3.11 shows an abnormal proliferation of hepatocytes on the surface of the organ. We considered this change as tumorigenesis. Figure 3.12, Figure 3.13 and Figure 3.14 show Sirius red stained liver sections revealing fibrogenesis around hepatic vein, arteriole and gall bladder,

respectively. We can observe thickened wall of blood vessel in chronically TAA treated liver (b) as compared to normal liver (a).

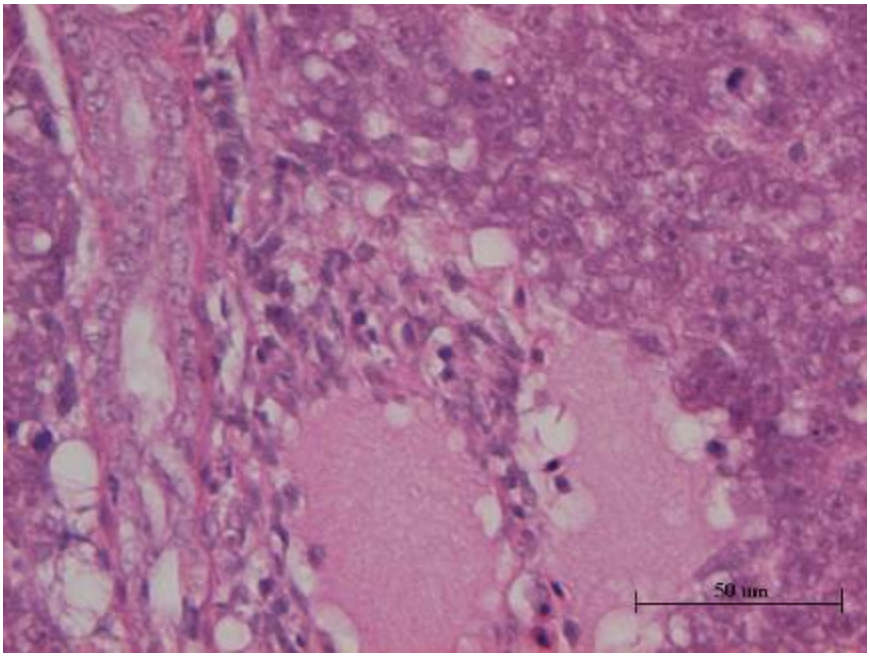

Figure 3.9 Inflammation in the liver of a medaka 14 days after 2 hours daily exposure to 0.4% TAA. The majority of these inflammatory cells are lymphocytes, which are generally smaller, with the cell nuclei smaller and darker than those of hepatocytes.

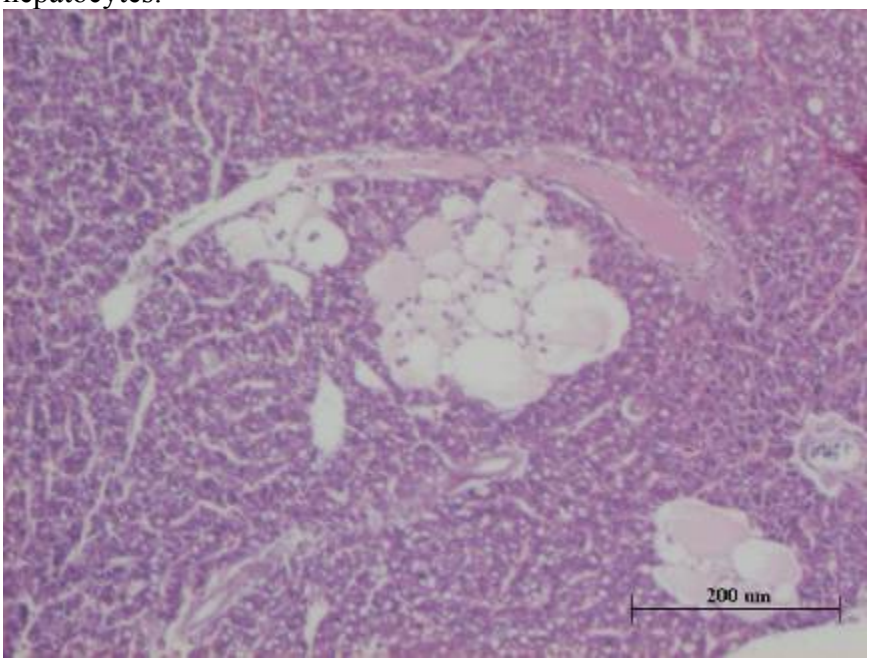

Figure 3.10 Spongiosis hepatis in the liver of a medaka 14 days after 2 hours daily exposure to 0.4% TAA. Spongiosis hepatis consists of multilocular cyst-like structures containing granular or flocculent eosinophilic material and occasionally erythrocytes.

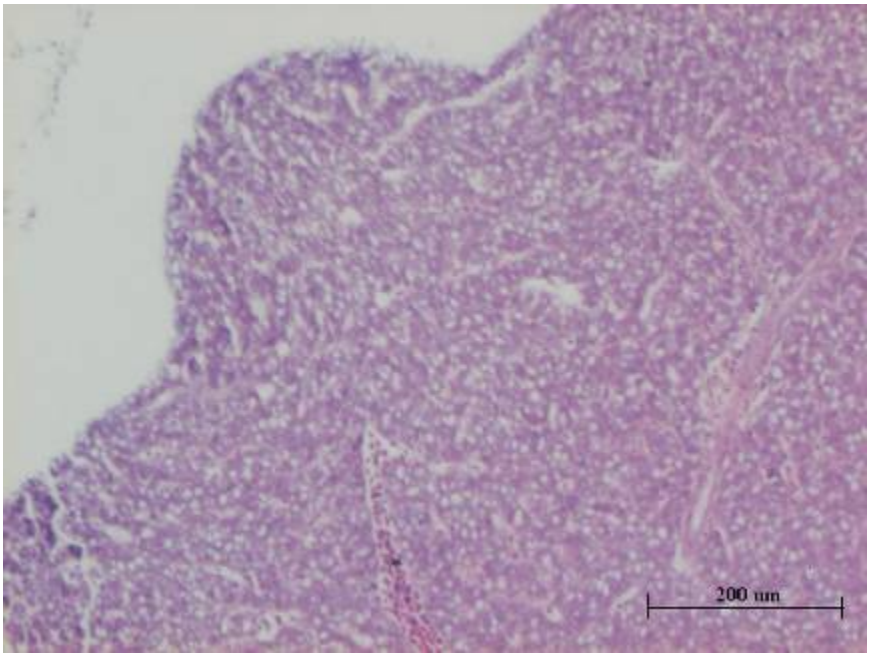

Figure 3.11 Tumorigenesis in the liver of a medaka 14 days after 2 hours daily exposure to 0.4% TAA.

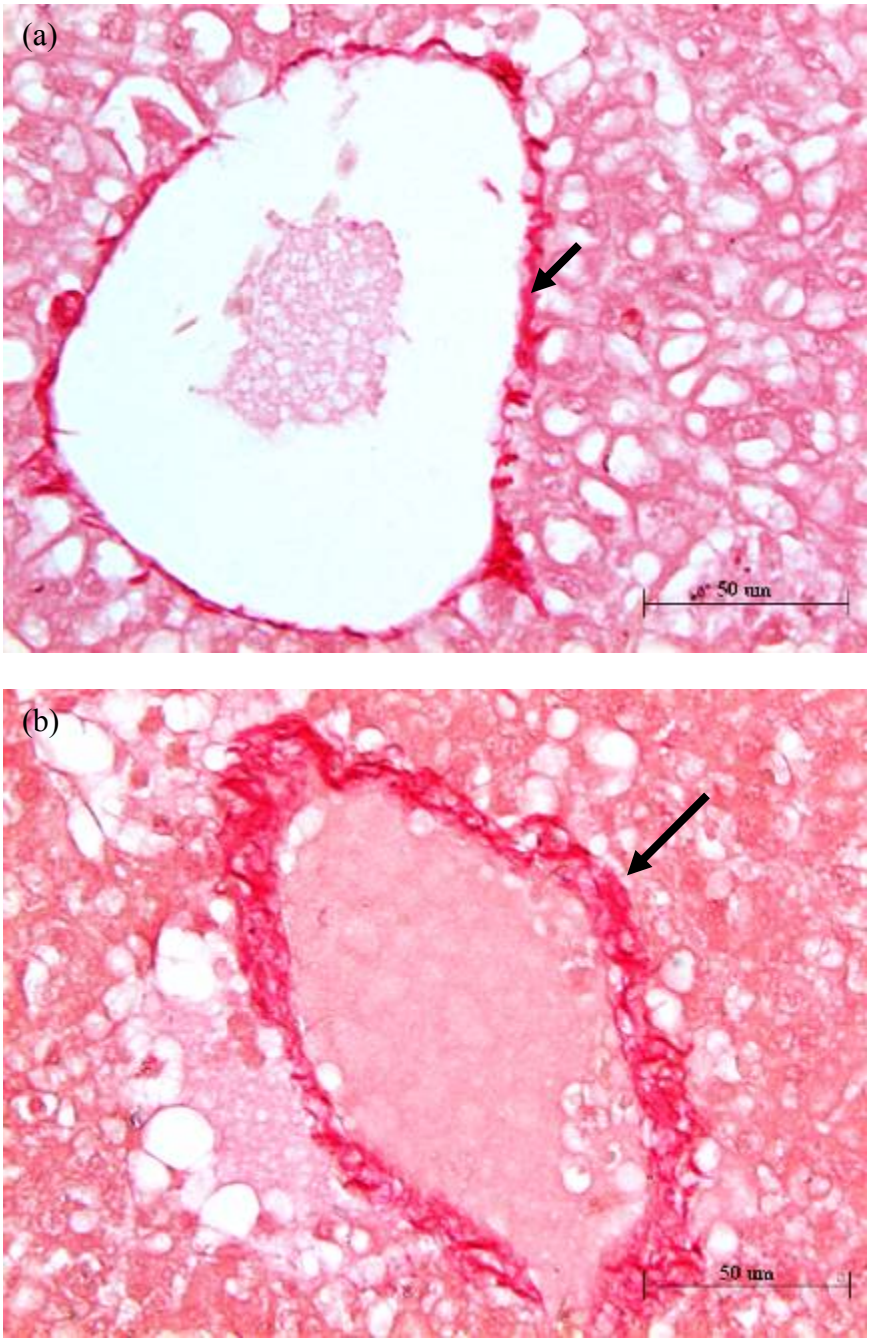

Figure 3.12 Hepatic veins in normal liver (a) and the damaged liver (b) 14 days after exposure to 0.4% TAA for 2 hours daily. The wall of blood vessel (bright red) is thicker in figure b (long arrow) than in figure a (short arrow).

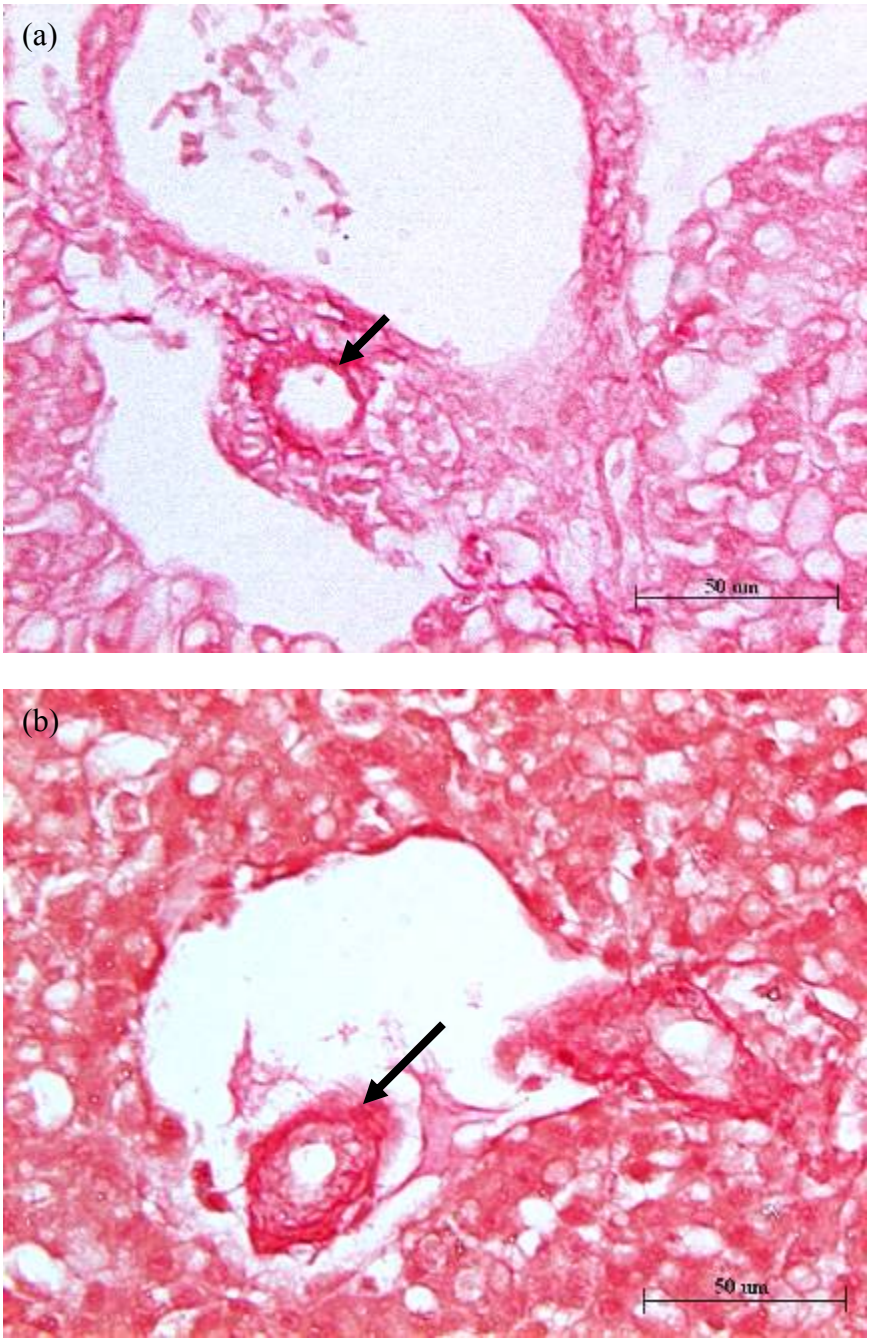

Figure 3.13 Hepatic arterioles in normal liver (a) and the damaged liver (b) 14 days after exposure to 0.4% TAA for 2 hours daily. The wall of blood vessel (bright red) is thicker in figure b (long arrow) than in figure a (short arrow).

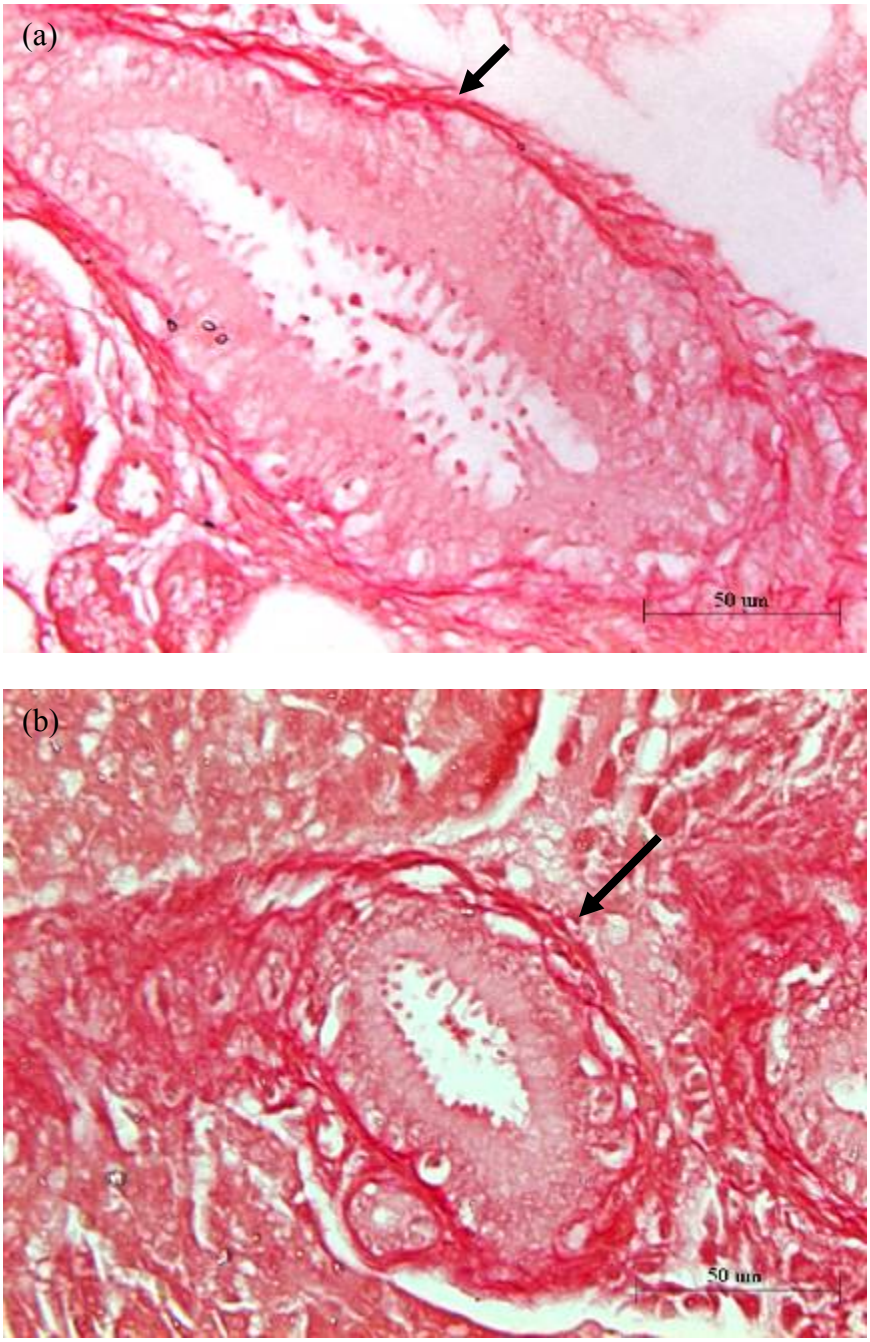

Figure 3.14 Gall bladders in normal liver (a) and the damaged liver (b) 14 days after exposure to 0.4% TAA for 2 hours daily. The wall of gall bladder (bright red) is thicker in figure b (long arrow) than in figure a (short arrow).

We have also examined the liver sections of medaka fish 7 days after exposure to 0.2% and 0.4% TAA for 14 hours every two days, see Figure 3.15. In 14 hours TAA treated medaka liver (Figure 3.15 c,d, e and f), the normal hepatic architecture was disrupted by

multifocal random areas of hepatocellular necrosis and loss in which many hepatic cords were replaced by irregular large, cystic spaces. These cystic spaces were lined by flattened cells and contained small numbers of swollen, sloughed, necrotic cells. Hepatocytes are severely swollen due to multiple small or single large clear cytoplasmic vacuoles. There is marked compression of sinusoidal spaces. The severity of liver degeneration is higher in 0.4% TAA treated fish (Figure 3.15 e and f) than 0.2% TAA treated fish (Figure 3.15 c and d).

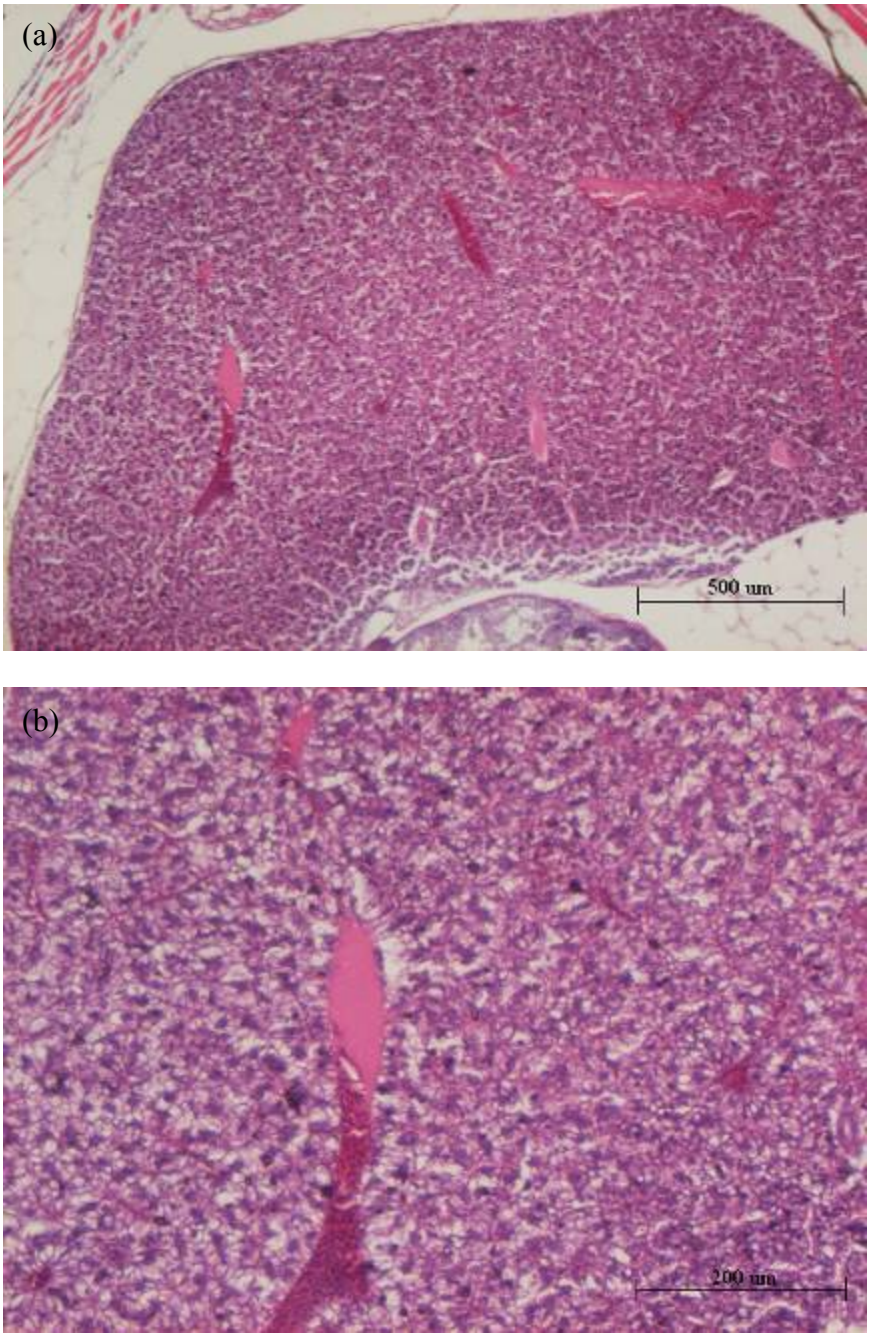

Figure 3.15 H&E stained liver sections from normal medaka fish (a, b), medaka fish exposed to 0.2% TAA for 14 hours every two days (c, d), and medaka fish exposed to 0.4% TAA for 14 hours every two days (e, f). a, c and e under magnification of 4x objective; b, d and f under magnification of 10x objective. In 14 hours TAA treated medaka liver (c,d, e and f), the normal hepatic architecture was disrupted by multifocal random areas of hepatocellular necrosis and loss in which many hepatic cords were replaced by irregular large, cystic spaces. There is marked compression of sinusoidal spaces. The severity of liver degeneration is higher in 0.4% TAA treated fish (e and f) than 0.2% TAA treated fish (c and d).

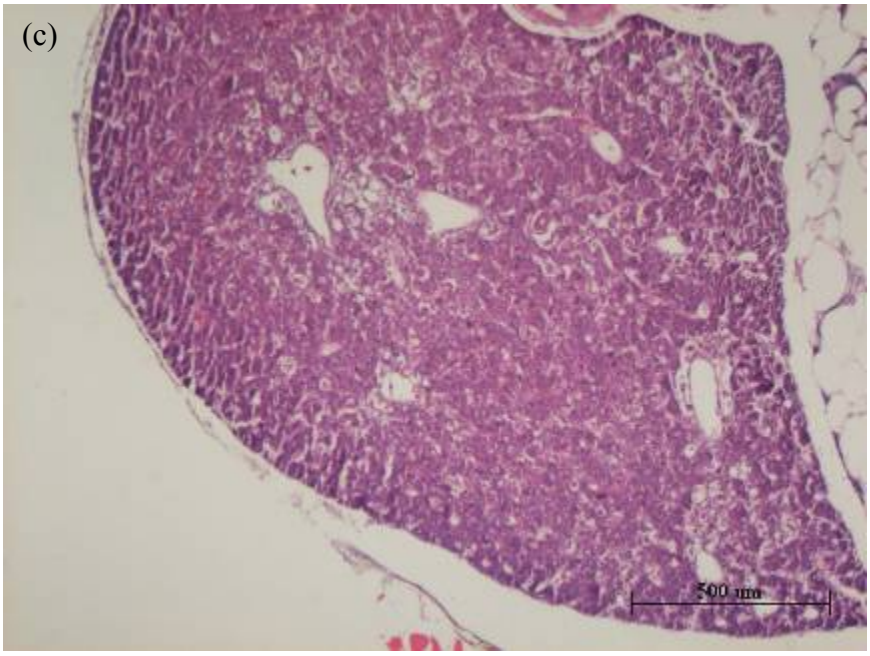
(c)
500 um

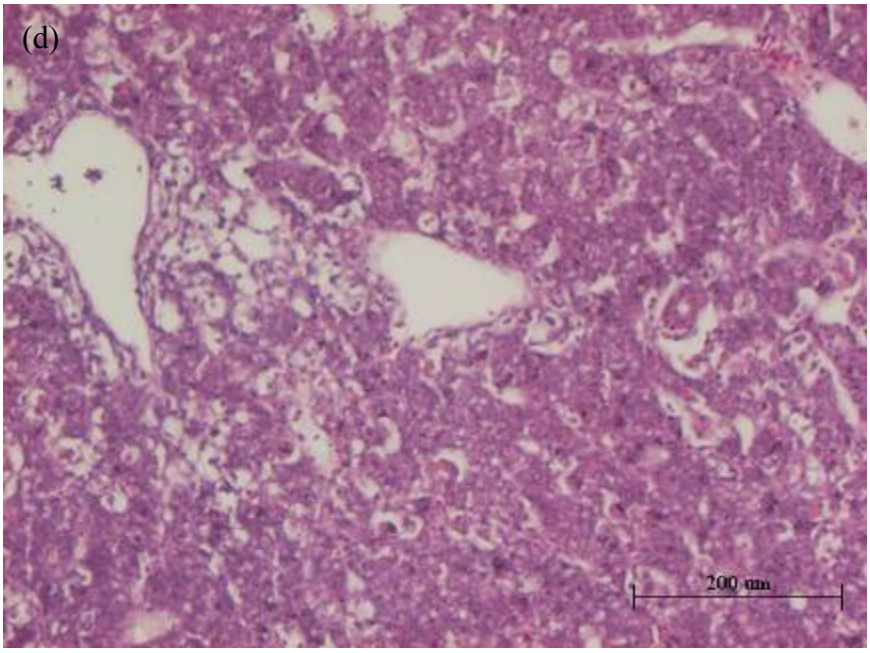
(d)
200 um

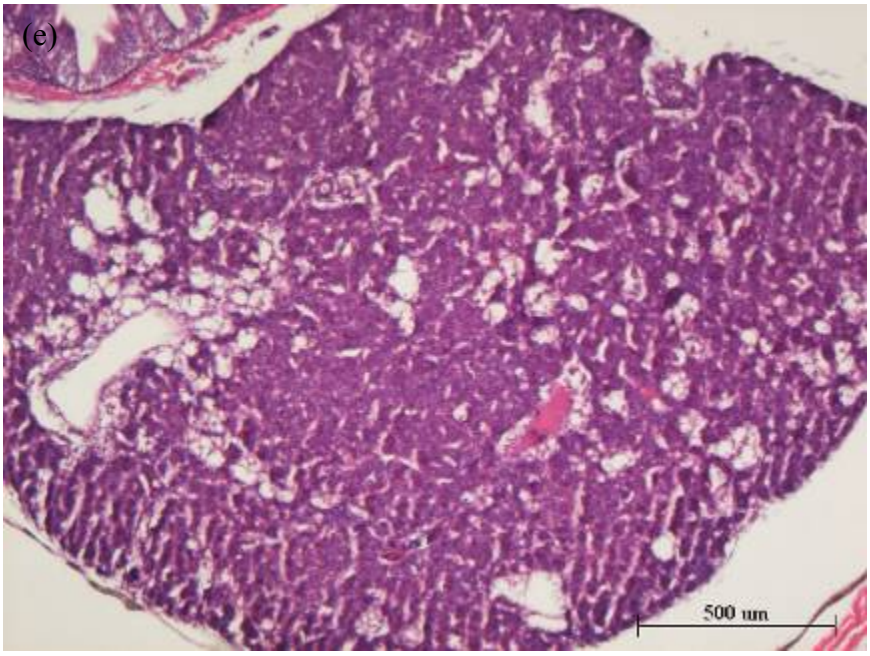

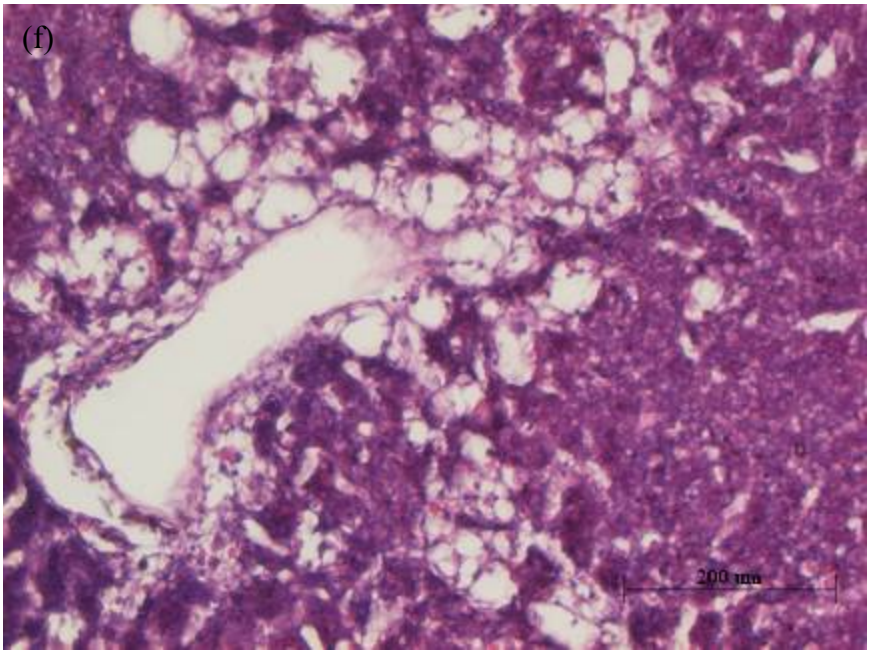

3.5 Liver tissue imaging by TPEF/SHG microscopy

SHG has been used to image the primary fibrillar collagens extensively. It is sensitive to structure as well as chemical composition. It has been verified that SHG signal readily image a highly subpopulation of collagen I and do not image elastin, collagen IV or other

basement membrane components (Brown et al, 2003). Thus SHG was used to image fibrillar collagen of ECM in liver, which is a primary indicator of liver fibrosis. TPEF results from the nonlinear excitation of molecular fluorescence. Excited with femtopulse laser, intrinsic molecules abundantly existed in hepatocytes plasma, such as NADH and flavins, emit fluorescence with substantial strength, making TPEF suitable for cell morphology observation in liver (Zipfel et al, 2003). The nuclear, the lipid droplet and the vacuole formed by degenerated hepatocytes appear dark in the TPEF image due to the lack of the fluorescence molecules. SHG/TPEF was used to image the collagen and hepatocyte simultaneously to show changes in fibrillar collagen as well as the hepatocyte morphology.

Figure 3.16 shows changes in collagen and cell morphology during liver damage. TPEF signal from hepatocytes was labeled with red pseudocolor, and SHG signal from collagen was labeled with green pseudocolor. In normal liver slice (Figure 3.16 a and b), there is no collagen aggregation, and all cells are arranged tightly with little gaps (back area). In the liver slice of a medaka fish exposed to 0.4% TAA (Figure 3.16 c and d), hepatocyte balloon degeneration (short arrow) and accumulation of fibrillar collagen (long arrow) were observed. These results can be used to indicate the information of pathological process of liver degeneration and liver fibrosis.

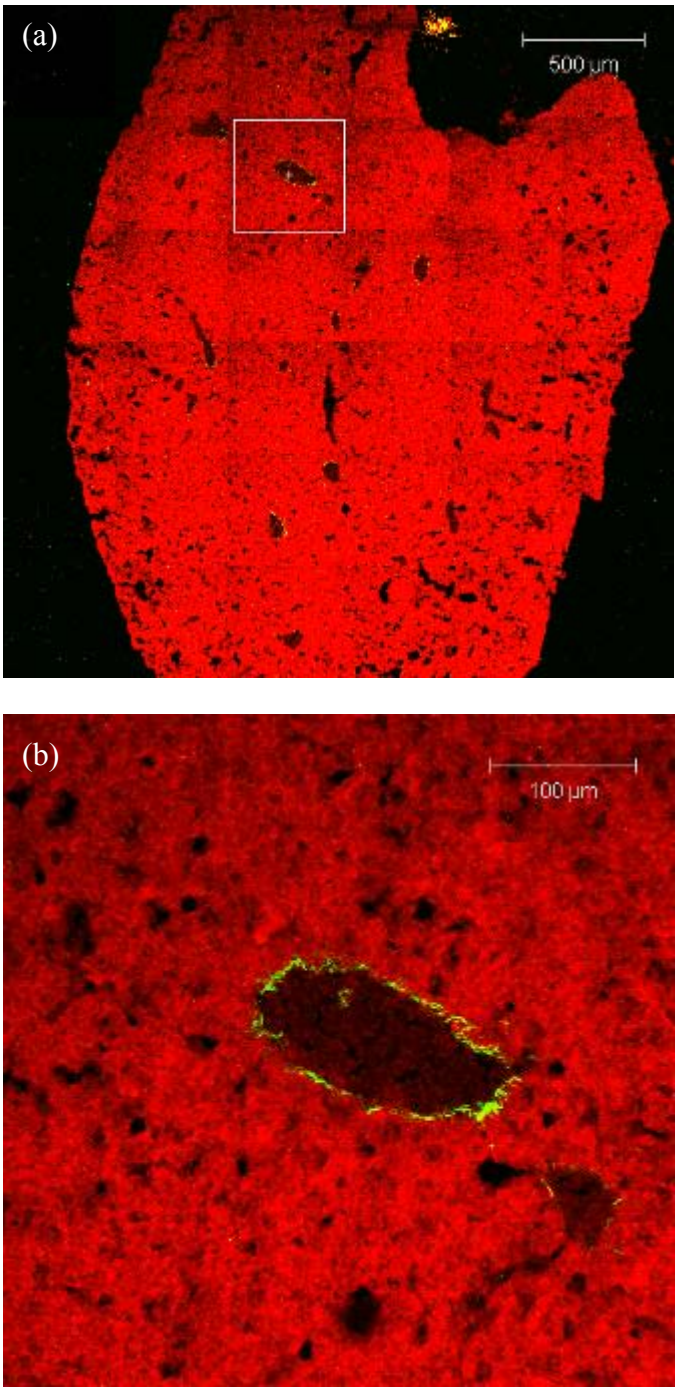

Figure 3.16 TPEF/SHG images of unstained liver sections from normal fish (a and b) and fish 14 days after exposure to 0.4% TAA (c and d). TPEF signal from hepatocytes was labeled with red pseudocolor, and SHG signal from collagen was labeled with green pseudocolor. Images of large area (a and c) were obtained by tile scan. Single images (b and d) were taken by 20x objective. In normal liver slice (a and b), there is no collagen aggregation, and all cells are arranged tightly with little gaps (back area). In the liver slice of a medaka fish exposed to 0.4% TAA (c and d), hepatocyte balloon degeneration (short arrow) and accumulation of fibrillar collagen (long arrow) were observed.

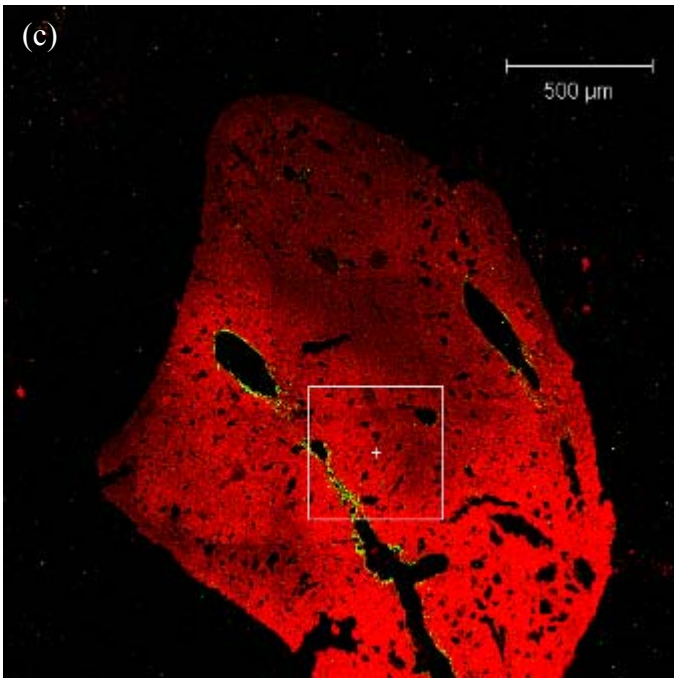

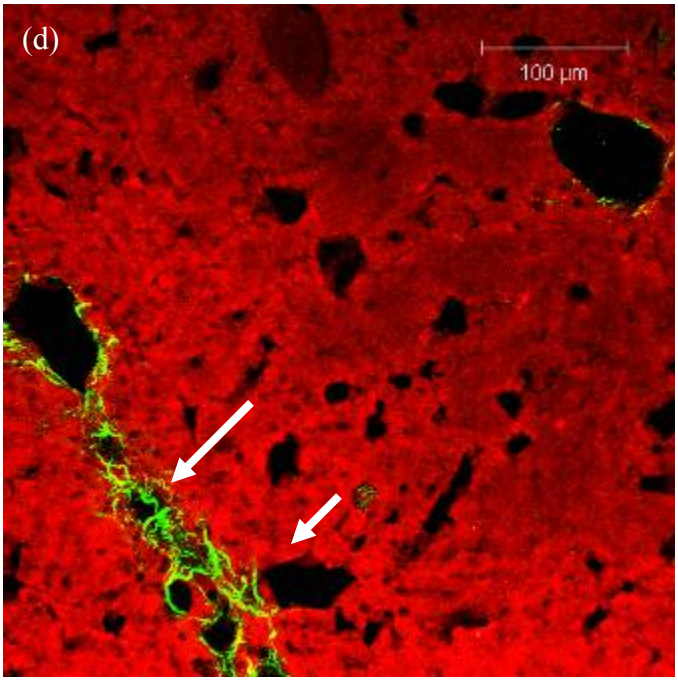

3.6 Quantitative analysis of liver damage

The amount of collagen and cell necrosis reflects the severity of liver damage. The TPEF/SHG images from unstained liver slice enable us to do quantitative analysis. Quantitative characterization produces more accurate description of the progression or

regression of liver damage, which is critical to evaluate the effectiveness of treatment or drug screening.

For quantification of collagen amount, images of SHG signal were processed to remove background noise and calculated the total intensity, by the algorithm described in Section 2.11. The whole process is illustrated in Figure 3.17. Figure 3.17a is the original gray scale image from SHG channel. The mask image (Figure 3.17b) is a binary image obtained by threshold segmentation. Figure 3.17c is the result of multiplying Figure 3.17a and Figure 3.18b, in which the background is set to zero. Line profiles (marked with lines) from the original image (Figure 3.17a) and processed image (Figure 3.17c) are shown in Figure 3.17d and Figure 3.17e, respectively. We can see that the noisy background has been removed while the objects are kept unchanged. The total intensity in Figure 3.17c is calculated and a number is generated for quantification. In Figure 3.18, we compared the collagen content in normal liver and 0.4% TAA-treated liver. A significant increase in collagen content was detected in damaged liver. To obtain statistically significant data, six 30 μm thick slices were scanned for each sample and three images were scanned for each slice under 20x objective. These results demonstrate that collagen amount can be quantified with high sensitivity from SHG signals.

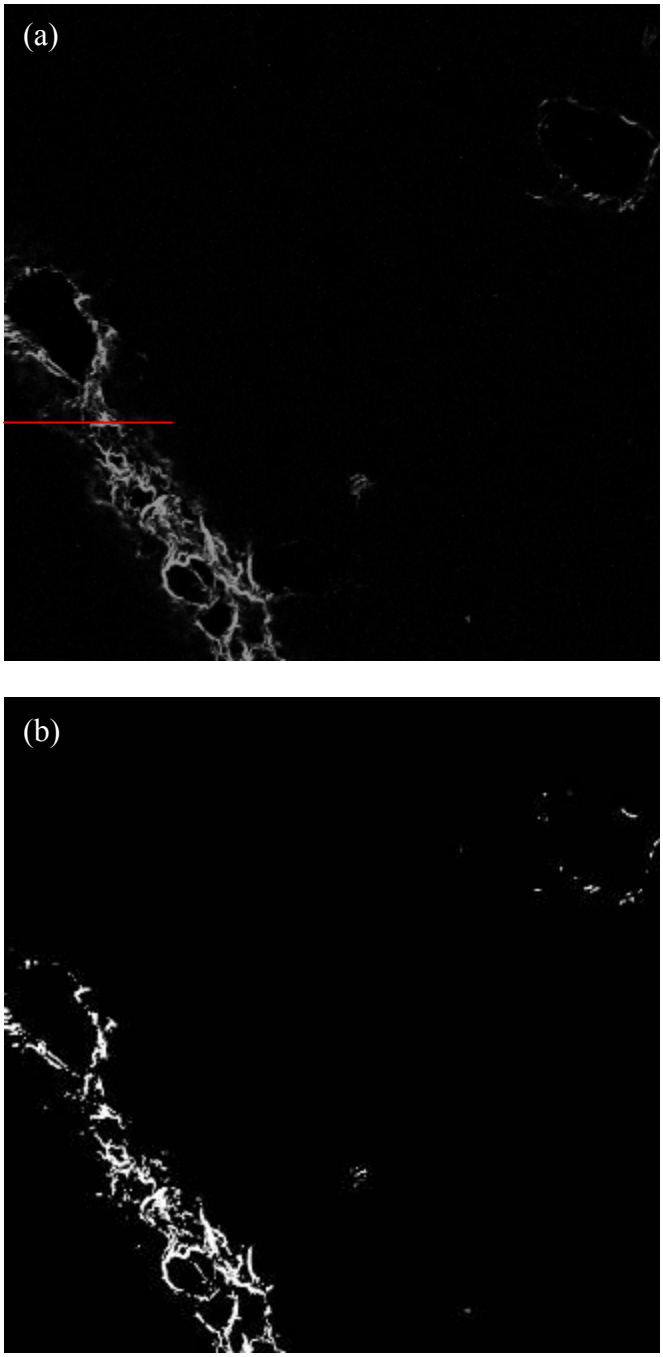

Figure 3.17 Image processing for background noise removal. The acquired gray images (a) were first segmented through Otsu thresholding. The obtained binary mask image (b) was then multiplied to the original image (a) and produced the final image (c) with removed background noise. The line profiles (d) and (e), extracted from the line marked in (a) and (c) respectively, shows the algorithm remove the background efficiently while keeping the signal intact.

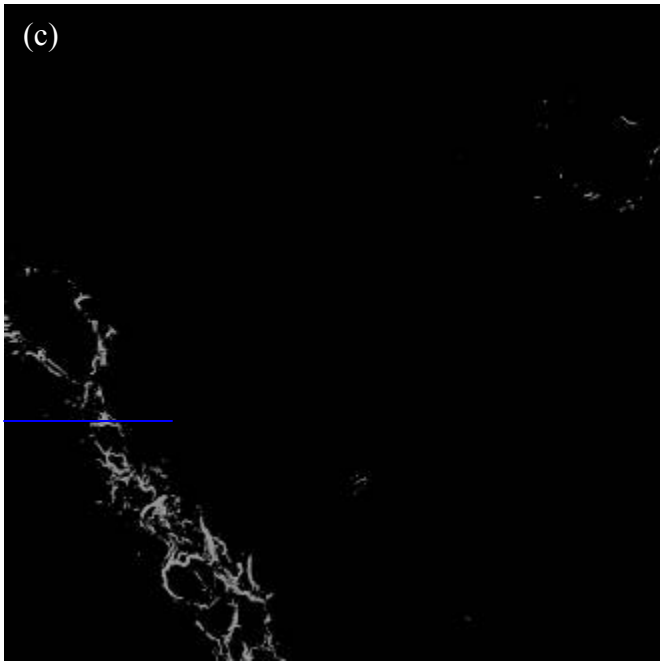
(c)

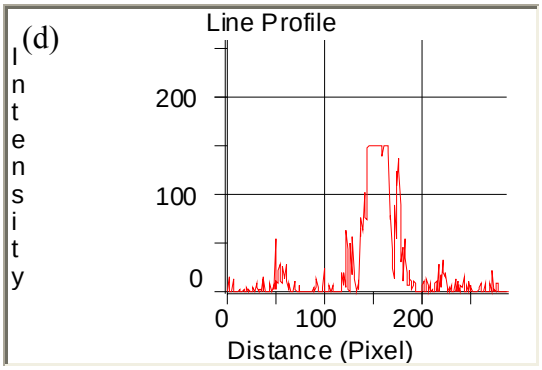
(d)
Line Profile
Intensity
200
100
0
0
100
200
Distance (Pixel)

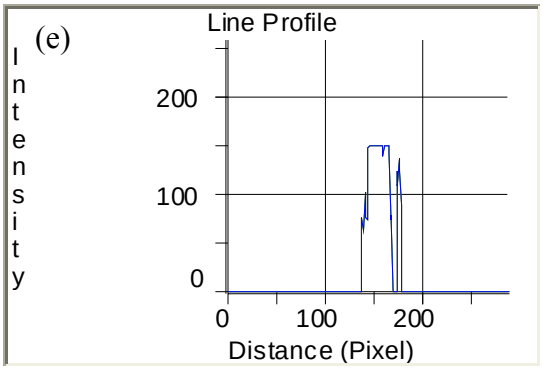
(e)
Line Profile
Intensity
200
100
0
0
100
200
Distance (Pixel)

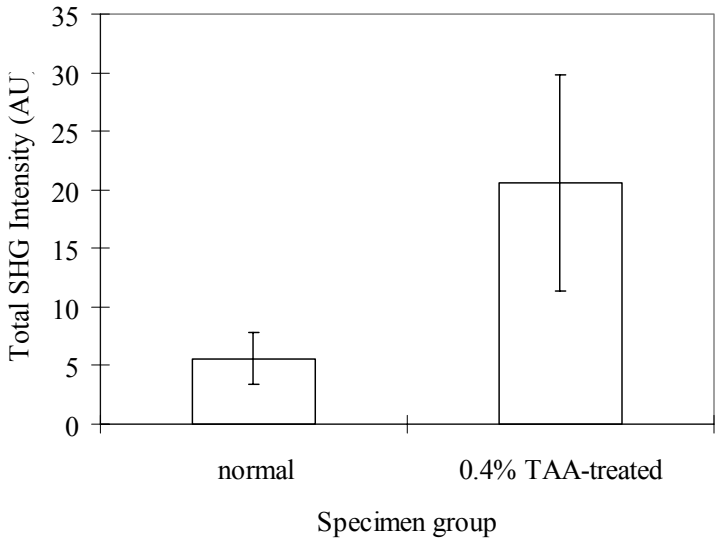

Figure 3.18 Quantification of collagen in normal liver and damaged liver 14 days after exposure to 0.4% TAA. Collagen content increased in the TAA treated liver compared to normal liver.

For quantification of cell necrosis, the area of dark regions in TPEF images is a measure of cell damage. To quantify it, the gray-scale TPEF images (Figure 3.19a) were first smoothed by low pass filter, followed by threshold segmentation, erosion and dilation. The resulted binary image is shown in Figure 3.19b. Area and aspect ratio of each object were then calculated. The objects were filtered by their areas. Blood vessels are normally large and regular in shape. They were ruled out in cell damage analysis. Only regions marked with pink color in Figure 3.19c were used to quantify cell damage and results are shown in Figure 3.20. Compared with normal liver, the 0.4% TAA-treated livers show significant cell damages. These results suggest that the area of cell necrosis in TPEF images can be used to quantify the severity of liver damage.

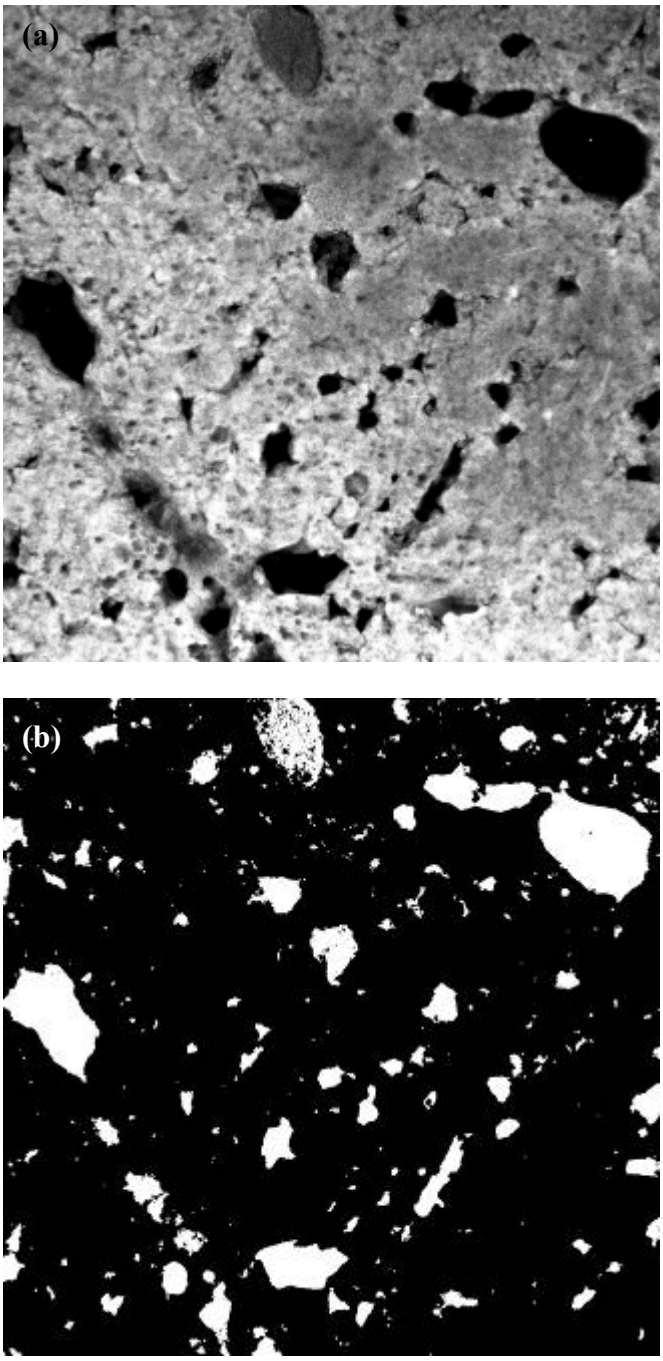

Figure 3.19 Image processing for quantification of cell damage. The acquired gray images (a) were smoothed by low pass filter, segmented through Otsu thresholding, eroded and dilated. The objects in the obtained binary mask image (b) were then calculated for area and aspect ratio. Large areas, which are regarded as blood vessels, were filtered out. Only pink areas shown in (c) were counted for cell damage.

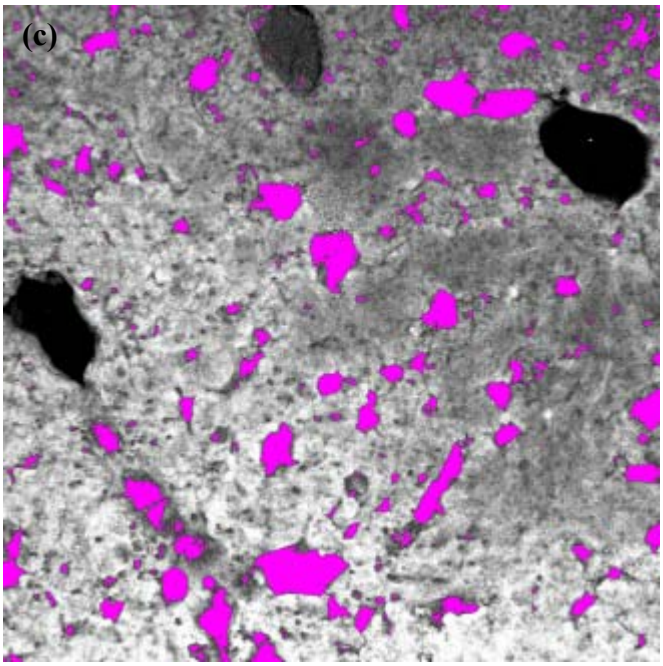

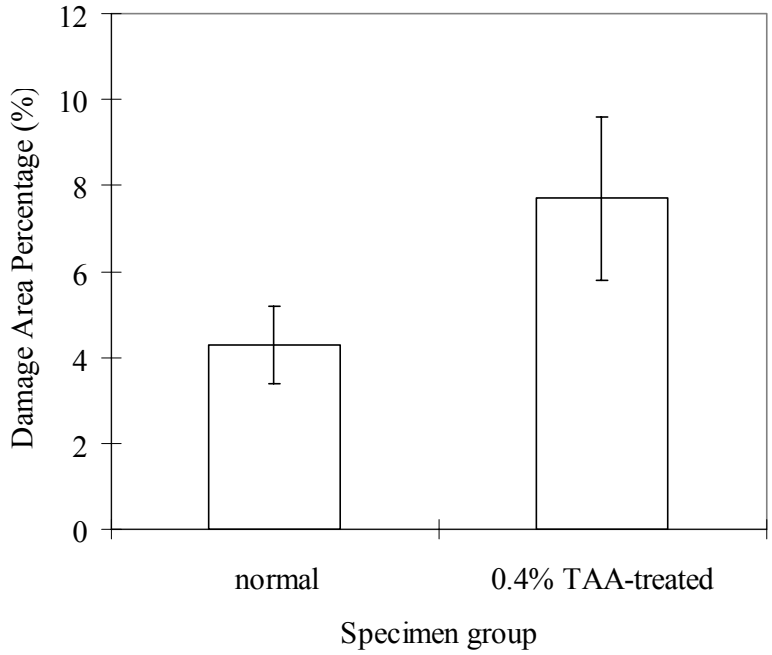

Figure 3.20 Quantification of cell necrosis in normal liver and damaged liver 14 days after exposure to 0.4% TAA. The percentage of damaged area is much higher in the TAA treated liver compared to normal liver.

3.7 3D imaging of RFP transgenic medaka liver

The liver-RFP transgenic fish which was first generated in zebrafish (Her et al, 2003) has been generated in Medaka by promoters of liver-type fatty acid binding protein (L-FABP) directing red fluorescence protein (RFP) in Dr. Hong Yunhan's lab. Figure 3.21 is a picture of adult transgenic fish taken by stereo microscope. The liver expresses strong red fluorescence signal under excitation of UV light.

Figure 3.21 Adult transgenic fish expressing RFP in the liver.

TPEF microscopy has intrinsic optical section ability and deep penetration depth. We have used it to image the whole unsectioned RFP liver. Whole liver was taken out from a normal liver-RFP transgenic medaka fish and fixed in 4% PFA. Without any further processing, the liver was put on a glass coverslip and imaged under TPEF microscope. Figure 3.22 illustrates the 3D stack images of RFP liver. Extremely high signal to noise ratio and subcellular resolution was achieved. Individual cell boundary, hepatic veins and sinusoids can be clearly visualized in 3D manner. The image depth can reach 100 μm with good resolution. Because no sample preparation (e.g., freezing, embedding or sectioning) was needed, the cell morphology and liver structure was perfectly preserved.

By developing proper imaging processing algorithm, the morphological and architectural changes can be analyzed in damaged liver. These analyses will facilitate high-throughput screening and can be a good tool for mechanism study. These images also demonstrate the ability of TPEF microscopy for high-resolution deep tissue imaging.

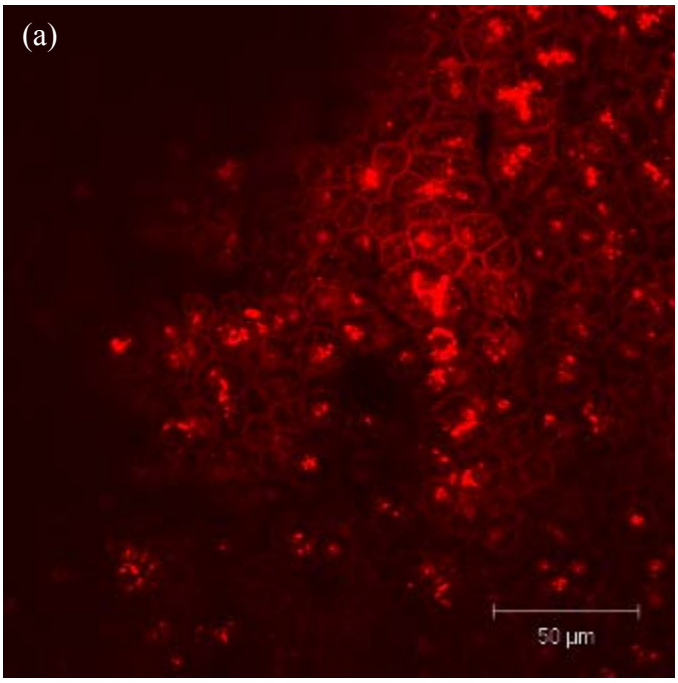

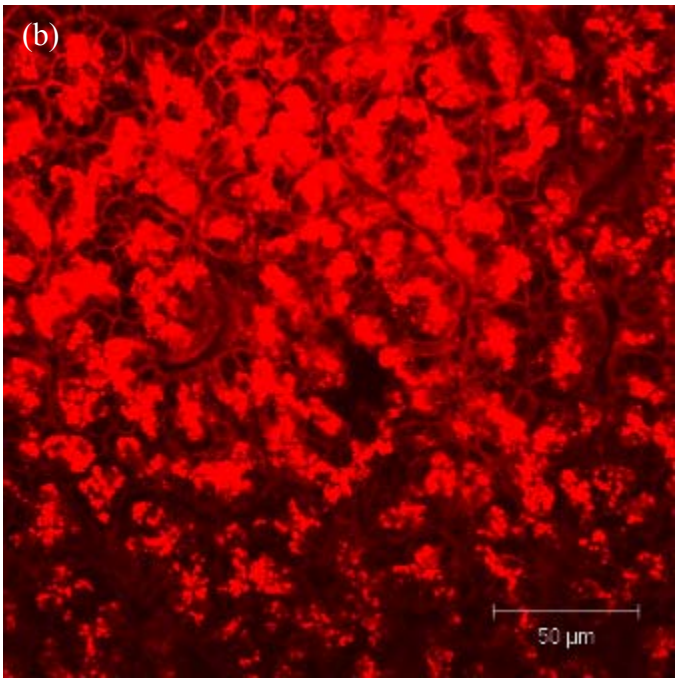

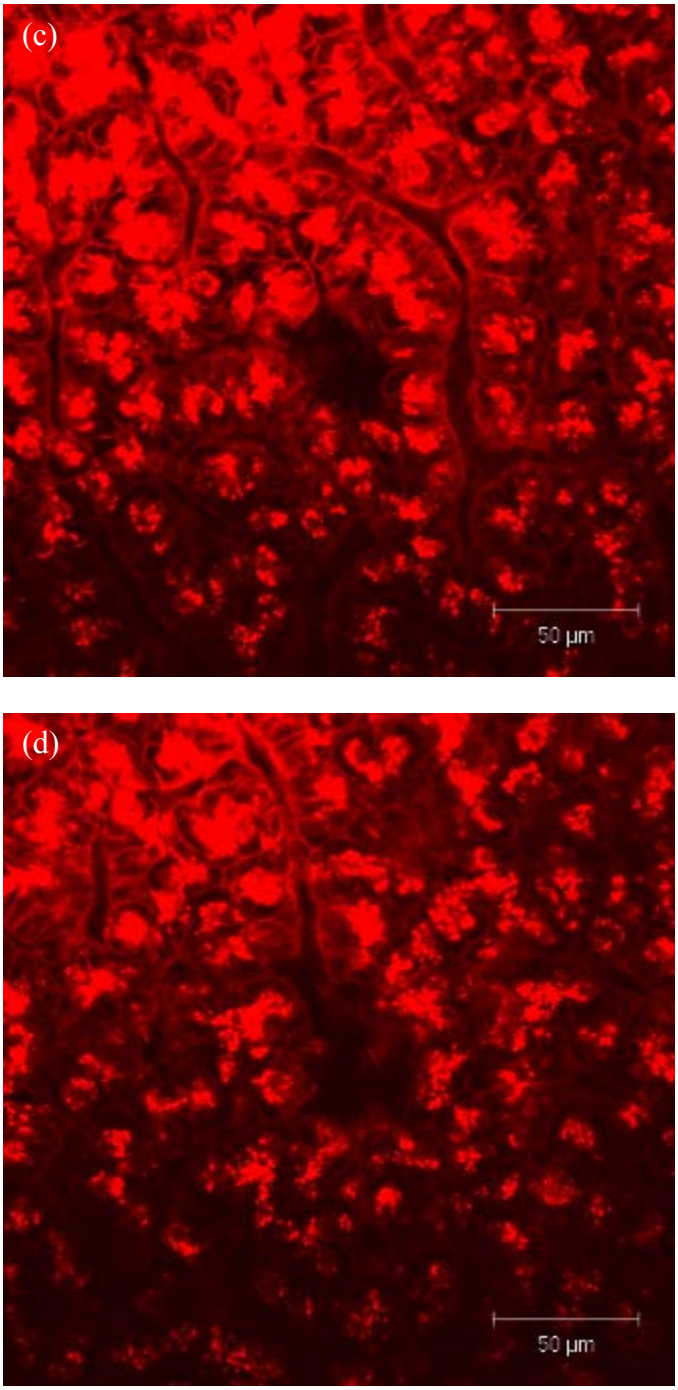

Figure 3.22 Deep tissue imaging of RFP-labeled liver. (a), (b), (c) and (d) were taken at the depth of 5 µm, 15 µm, 20 µm and 30 µm, respectively from the organ surface. The cell morphology and arrangement, hepatic vein and sinusoidal structure can be observed with high resolution at different layers.

3.8 Image depth enhancement by optical clearing

Image depth is one of the key parameters for deep tissue imaging. We have investigated

ways of improving image depth in turbid tissue. Optical clearing by application of biocompatible and hyperosmotic agents such as glycerol has been commonly used to improve the imaging depth into highly scattering tissue (Cicchi and Pavone, 2005). In this study, we treated the specimen of fresh tissue with 50% glycerol and observed great imaging depth enhancement using two-photon microscopy. We also investigated the effect of freezing of the glycerol treated sample on imaging depth and observed equivalent improvement of penetration depth as the fresh glycerol treated sample. The results are plotted in Figure 3.23. The mechanism of optical clearing with glycerol treatment was suggested to result from refractive index match and dehydration (Wang et al, 2003). For the frozen sample, the mechanism needs to be investigated. By examining the optical clearing effect of freezing, it could be useful for cryosurgery and a number of optical therapeutic and diagnostic applications, and moreover, for 3D reconstruction of the whole organ in our future project.

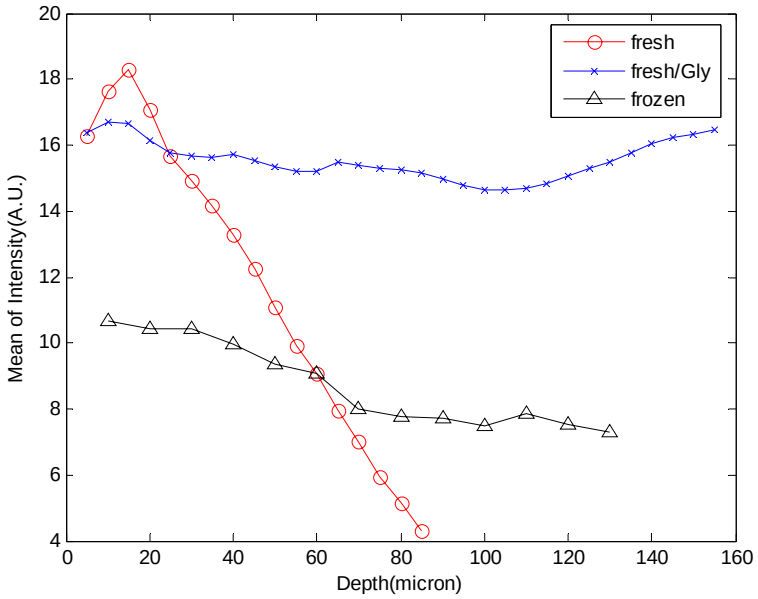

Figure 3.23 Image depth enhancements by glycerol and frozen treatment. The mean intensity along tissue depth have been improved in glycerol treated fresh ('x') and frozen (triangle) samples compare to untreated sample (circle).

CHAPTER 4 DISCUSSION

4.1 Medaka model of hepatotoxicity and liver fibrosis

Medaka is a good model to study hepatotoxicity. The liver is the largest abdomen organ in medaka and resembles mammalian liver in many features. It has major types of cells existing in mammalian liver, and has similar vascular and parenchymal relationships as mammalian liver; although there are some differences in anatomic feature (see Figure 3.1 ~ Figure 3.3).

We have applied TAA, one of the most commonly used hepatic toxins, to study the toxic response of medaka liver. TAA is proven to be very effective in causing liver damage in medaka liver. A few pathological changes, including inflammation, cell necrosis, spongiosis, fibrosis and tumorigenesis, were observed in TAA treated medaka liver (Figure 3.7 ~ Figure 3.15). Individual fish may have different response or severity of damage after exposure to TAA. It is due to different metabolic rate or the intrinsic complexity of in vivo model. This problem can be minimized by using the same batch of fish or by increasing the sample number to get statistical results, which is very practical for medaka as compared to mammalian models.

The way of administrating TAA also played an important role in causing different liver damage. TAA was administrated in water and received by oral ingestion. The parameters we can play with are the TAA concentration, treatment period, frequency and total treatment time. We have designed two treatment schemes with varying TAA

concentration. The most effective concentration under each treatment scheme was determined (Figure 3.4 and Figure 3.5). The chronic treatment was conducted by exposing fish to TAA 2 hours daily. The acute treatment was conducted by exposing fish to TAA 14 hours every two days. Chronic treatment tended to cause liver fibrosis and neoplasm (Figure 3.9 ~3.14), whereas acute treatment caused mainly cell necrosis (Figure 3.15). By varying the time parameters (period, frequency and duration) and finding out effective TAA concentration, we can expect to establish various liver disease models, such as steatosis, fibrosis, cirrhosis and neoplasia, using medaka fish.

In mice model, daily administration of 0.03% TAA in drinking water for 8 weeks will induce liver fibrosis. The amount of collagen in fibrosis liver would increase up to 6- fold as compared to that of normal liver (Fatima Teixeira-Clerc, et al., 2006). Although we observed an increase in collagen content after TAA treatment in medaka model, the increase was not as significant as that of mice model. The histological feature of fibrosis medaka liver was also not as obvious as that of mice model. These differences may result from their different anatomical features that the classic lobule structure with portal tract and central vein in mammalian liver does not exist in fish. Moreover, the uptaking and metabolic rate of foreign chemical are different in fish liver as compared to mammals. The TAA treatment time and duration in medaka model may need further optimization in order to achieve more comparable pathological results to mammalian model.

4.2 TPEF/SHG for quantitative tissue diagnosis

TPEF/SHG imaging is a more sensitive method than traditional histological staining.

Excited by femto-second pulse laser, the resolution and signal to noise ratio of TPEF/SHG microscopy is much higher than that of light microscopy. Moreover, signals of both TPEF and SHG were generated by the intrinsic molecules in the tissue. Thus no sample processing and staining are needed. The images were generated with low artifact. They are suitable for highly quantitative analysis. We have imaged 20 μm thick unstained cyrosectioned liver slices from both normal and TAA treated fish (Figure 3.16). High resolution images revealing collagen distribution and tissue architecture were obtained. The pathological changes including collagen deposition and cell necrosis were detected in TAA-treated fish liver. These results demonstrate that TPEF/SHG imaging is a very good tool to study hepatotoxicity and liver fibrosis with high sensitivity.

TPEF/SHG images are very suitable for quantitative analysis. We have developed image processing algorithms to quantify the collagen amount from SHG signal and the cell necrosis from TPEF signal (Figure 3.17 and Figure 3.19). We first eliminated the background noise by non-parametric algorithm, in which threshold for segmentation was calculated automatically. Then we generated mask images and filtered out unwanted area and signal. The mask images were finally used to calculate the SHG intensity and damaged area. These algorithms are non-parametric and quite robust. Using these methods, we have detected the changes quantitatively in collagen amount and cell necrosis between normal and TAA-treated fish (Figure 3.18 and Figure 3.20). Robust and sensitive algorithms are very essential for detection of subtle changes. Quantifying the subtle changes in liver tissue is not practical from the traditional histological images. This TPEF/SHG imaging system combined with robust image processing algorithm

demonstrates a higher effectiveness and sensitivity for tissue diagnosis and drug screening than any traditional method.

4.3 High resolution whole organ imaging of fish liver

The liver-RFP transgenic medada fish was produced by promoters of liver-type fatty acid binding protein (L-FABP) directing red fluorescence protein (RFP). This transgenic line has been stably established and propagated in the aquarium. By labeling hepatocytes with RFP, the contrast and signal to noise ratio of TPEF images have been greatly improved. In wild-type liver, the TPEF signal comes from the autoflorescence of intrinsic molecules. In order to obtain images with adequate intensity, we have to use high detector gain. The higher the detector gain, the lower the signal to noise ratio. For imaging of RFP labeled liver, the detector gain can be lowered when equivalent intensity is obtained. The image contrast can also be greatly improved by highlighting the RFP signal. We have taken three-dimensional images from an uncut whole RFP-labeled liver (Figure 3.22). The cell boundary and vascular structures deep in the tissue can be clearly identified. It is promising that the whole organ of RFP-labeled medaka liver can be constructed by two-photon tissue cytometry (Ragan et al, 2007) with subcellular resolution. By constructing the whole organ, we can have a thorough understanding of the microscopic structure of fish liver. Any phenotypic change in the liver cell and vascular structure can be detected with high sensitivity and resolution. The two photon imaging system together with the transgenic fish line will be a good platform to study hepatotoxicity and perform drug screening.

In order for the future application of deep tissue imaging and whole organ construction, we have investigated the penetration depth of TPEF imaging. Liver is a highly-scattering tissue. The penetration depth of TPEF microscopy is limited by the turbid nature of the tissue. A lot of investigations have been done to improve the imaging depth in turbid tissue by applying optical clearing agents such as glycerol. Besides using this established optical clearing method, we investigated the imaging depth on optical cleared frozen tissue, because freezing is necessary for easy cutting when we do whole organ imaging. The penetration depths of TPEF imaging on fresh, optical cleared fresh and frozen tissue have been investigated (Figure 3.23). Tremendous improvements on imaging depth have been observed in optically cleared samples. This investigation provides useful information and technical solution for our future work of whole organ imaging.

4.4 Future work

In this study, we determined the effective TAA concentration from the fish survival rate. Due to limited time and resource, TPEF/SHG imaging and quantitative analysis were only performed on liver tissue that treated by one of the effective concentrations. To further validate the sensitivity of the TPEF/SHG quantification method, it is necessary to perform quantitative analysis of liver damage and collagen deposition on samples subjected to increasing amount of TAA treatment, and to compare the image quantization results to the Realtime RT-PCR results.

REFERENCES

Amali A.A., et al. (2006). Thioacetamide induced liver damage in zebrafish embryo as a disease model for steatohepatitis. *Journal of Biomedical Science.* 13, 225-232.

Bataller R, Brenner DA (2005). Liver fibrosis. *J Clin Invest.* 115:209-18.

Brown E, et al. (2003). Dynamic imaging of collagen and its modulation in tumors in vivo using second-harmonic generation. *Nature Medicine.* 9, 796-800.

Cicchi R. and F.S. Pavone. (2005). Contrast and depth enhancement in two-photon microscopy of human skin ex vivo by use of optical clearing agents. *Optics Express*. 13, 2337-2344.

Cox G, et al. (2003). 3-Dimensional imaging of collagen using second harmonic generation. *Journal of Structural Biology*. 141, 53–62.

Dahab, G.M., et al. (2004). Digital quantification of fibrosis in liver biopsy sections: description of a new method by Photoshop software. *J Gastroenterol Hepatol*. 19**,** 78-85.

Farber, S. A. *et al.* (2001). Genetic analysis of digestive physiology using fluorescent phospholipid reporters. Science. 292, 1385–1388.

Fatima Teixeira-Clerc, et al. (2006). CB1 cannabinoid receptor antagonism: a new strategy for the treatment of liver fibrosis. *Nature Medicine.* 12, 671-676.

Henderson N. and Iredale P (2007). Liver fibrosis: cellular mechanisms of progression and resolution. *Clinical Science.* 112: 265-280.

Her GM, Chiang CC, Chen WY, Wu JL. (2003). In vivo studies of liver-type fatty acid binding protein (L-FABP) gene expression in liver of transgenic zebrafish (Danio rerio). *FEBS Letters*. 538, 125-133.

Hinton DE, Segner H, Braunbeck T (2001). Chapter 4. Toxic responses of the liver. In: *Target Organ Toxicity in Marine and Freshwater Teleosts. Volume 1 Organs* Edited by: *Schlenk D, Benson WH. London, Taylor and Francis*, 224-268.

Hodgson S, Harrison RF, Cross SS. (2006). An automated pattern recognition system for the quantification of inflammatory cells in hepatitis-C-infected liver biopsies. Image and Vision Computing. 24, 1025-1038.

Ishak KG, Zimmerman HJ. (1995). Morphologic spectrums of drug-induced liver disease. *Gastroenterol Clin North Am*. 24, 759.

Ishikawa, Y. (2000). Medakafish as a model system for vertebrate developmental genetics. *BioEssays* 22, 487-495.

Ju Z, Wells MC, Martinez A, Hazlewood L, Walter RB. (2005). An *in silico* mining for simple sequence repeats from expressed sequence tags of zebrafish, medaka, *Fundulus*, and *Xiphophorus*. *In Silico Biol.* 5(5–6), 439–463.

Lake-Bakaar G, Mazzoccoli V, Ruffini L. (2002). Digital Image Analysis of the Distribution of Proliferating Cell Nuclear Antigen in Hepatitis C Virus-Related Chronic Hepatitis, Cirrhosis, and Hepatocellular Carcinoma. Digestive Diseases and Sciences. 47, 1644-1648.

Langheinrich U. (2003). Zebrafish: a new model on the pharmaceutical catwalk. *BioEssays*. 25, 904-912.

Liu Z, Kullman SW, Bencic DC, Torten M, Hinton DE. (2003). ras oncogene mutations in diethylnitrosamine-induced hepatic tumors in medaka (*Oryzias latipes*), a teleost fish. *Mutat Res.* 539, 43–53.

Ma T, Wan X, Huang Q, Wang Z, Liu J. (2005). Biomarker responses and reproductive

toxicity of the effluent from a Chinese large sewage treatment plant in Japanese medaka (*Oryzias latipes*). Chemosphere 59, 281–288.

Masseroli, M., et al. (2000). Automatic quantification of liver fibrosis: design and validation of a new image analysis method: comparison with semi-quantitative indexes of fibrosis. *J Hepatol.* 32, 453-64.

Orifei E., 2003. Review of pathology of the liver, Department of Pathology, Stritch School of medicine, Loyola University of Chicago, http://www.meddean.luc.edu.

Otsu, N. (1979). A threshold selection method from gray level histograms. *IEEE Trans. System, Man and Cybernetics*. 9, 62-66.

Ragan T., et al. 2007. High-resolution whole organ imaging using two-photon tissue cytometry. *Journal of Biomedical Optics*. 12, 014015.

Rocha E, Monteiro A. F., and Pereira C. A. (1995). Microanatomical organization of hepatic stroma of the brown trout, Salmo trutta fario (Teleostei, Saomonidae): A qualitative and quantitative approach. *Journal of Morphology*. 223, 1-11.

Schnur J, et al. (2004). Thioacetamide-induced hepatic fibrosis in transforming growth factor beta-1 transgenic mice. Eur J Gastroenterol Hepatol. 16,127–133.

Scholz S, Kordes C, Hamann J, Guizeit HO. (2004). Induction of vitel-logenin *in vivo* and *in vitro* in the model teleost medaka (*Oryzias latipes*): comparison of gene expression and protein levels. *Mar Environ Res.* 57, 235–244.

Schuster D, Laggner C and Langer T. (2005). Why Drugs Fail – A Study on Side Effects in New Chemical Entities. *Current Pharmaceutical Design*, 11, 3545-3559.

Serra, J. (1982). Image Analysis and Mathematical Morphology. London, New York: Academic Press.

Shimada A, Shima A, Nojima K, Seino Y, Setlow RB. (2005). Germ cell mutagenesis in medaka fish after exposures to high-energy cosmic ray nuclei: a human model. *Proc Natl Acad Sci USA*. 102, 6063–6067.

So P. T. C. and Kim H. (1998) Two-photon deep tissue ex vivo imaging of mouse dermal and subcutaneous structures. *Optics Express.* 3, 339-350.

Wang K., Xu X., He Y. and Elder J.B. (2003). Investigation of Optical Clearing of Gastric Tissue Immersed With Hyperosmotic Agents. *IEEE JOURNAL OF SELECTED TOPICS IN QUANTUM ELECTRONICS*. 9, 234-242.

Winn RN, Kling H, Norris MB. (2005). Antimutagenicity of green tea polyphenols in the liver of transgenic medaka. *Environ Mol Mutagen.* 46, 88–95.

Wittbrodt, J., Shima, A. and Schartl, M. (2002). Medaka – a model organism from the Far East. *Nature Reviews Genetics* 3**,** 53-64.

Wu J, Zern M.A (2000). Hepatic stellate cells: a target for the treatment of liver fibrosis. *J Gastroenterol.* 35: 665-672.

Zimmerman HJ. (1998). Drug-induced liver disease. In Schiff ER, Sorrell MF, Maddrey WC, eds. Diseases of the liver. Philadelphia: JB Lippincott, 973-1964.

Zimmerman HJ. (1999). Chapter 10. Indirect Cytotoxic Hepatotoxins. In: Hepatotoxicity. Lippincott Williams&Wilkins, 266-267.

Zipfel W.R., et al. (2003). Live tissue intrinsic emission microscopy using multi-photon excited native fluorescence and second harmonic generation. *Proc Natl Acad Sci U S A.* 100, 7075-7080.

Zon LI, Peterson RT. (2005). In vivo drug discovery in the zebrafish. *Nat Rev Drug Discov.* 4, 35-44.